Analysis of Asymmetric Dual-Hop Energy Harvesting-Based Wireless Communication Systems in Mixed Fading Environments

Elmehdi Illi, *Member, IEEE,* Faissal El Bouanani, *Senior Member, IEEE,* Paschalis C. Sofotasios, *Senior Member, IEEE,* Sami Muhaidat, *Senior Member, IEEE,* Daniel Benevides da Costa, *Senior Member, IEEE,* Fouad Ayoub, *Member, IEEE,* and Ala Al-Fuqaha, *Senior Member, IEEE*

***Abstract*—This work investigates the performance of a dual-hop energy harvesting-based fixed-gain amplify-and-forward relaying communication system, subject to fading impairments. We consider a source node (S) communicating with a destination node (D), either directly or through a fixed distant relay (R), which harvests energy from its received signals and uses it to amplify and forward the received signals to D. We also consider maximal-ratio combining at D to combine the signals coming from S and R. Both power-splitting and time-switching energy harvesting protocols are investigated. The S-R link is modeled by Nakagami-m fading model, while the R-D and S-D links experience α-μ fading. Closed-form expressions for the statistical properties of the total signal-to-noise ratio are derived, based on which novel closed-form expressions are then derived for the average symbol error rate as well as for the average channel capacity, considering four different adaptive transmission policies. The derived expressions are validated through Monte Carlo simulations.**

***Index Terms*—Adaptive transmission policies, amplify-and-forward, energy harvesting, diversity, fading channels.**

I. Introduction

The ever-increasing demand for broadband communication systems and the growing number of connected devices are the driving forces for the evolution of wireless technologies in the past decades [1]. With the emergence of new paradigms such as the Internet of Things (IoT) as well as machine-to-machine (M2M) communication, the next generation of wireless networks is envisioned to catalyze the wide deployment of new technologies and services, such as remote healthcare, surveillance, and transportation [2].

In addition to the need for higher data rates and expansion of network coverage, the maximization of the energy efficiency is among the most critical challenges for the fifth generation (5G) of wireless networks and beyond [3], where the power consumption and battery lifetime of wireless nodes are of paramount importance [1], [4]. Although energy resources (e.g., battery) are limited, the connected devices in 5G systems are envisaged to operate in multiple spectrum bands, as well as providing real-time processing [5]. Additionally, M2M devices and wireless sensors are typically deployed in difficult-to-reach areas, e.g., structural health monitoring and mine tunnels [5], [6], making the battery recharging or replacement impractical in most cases.

Recently, energy harvesting (EH) has emerged as an attractive solution that is envisioned to provide a greener and sufficient energy supply to self-sustainable wireless commutations [7]. Radio-frequency energy harvesting (RF-EH) was proposed recently as a promising solution to provide perpetual energy replenishment for wireless networks. RF-EH is realized by allowing wireless devices, equipped with dedicated EH circuits, to harvest energy from either ambient RF signals or dedicated RF sources [8], [9]. In M2M communications and wireless sensor networks (WSN), terminal nodes harvest energy from either access points or dedicated power sources/base stations [1]. RF-EH can be categorized into two main strategies, namely, (i) wireless-powered communications (WPC) [10] and (ii) simultaneous wireless information and power transfer (SWIPT), which has been shown to provide noticeable gains in terms of power and spectral efficiencies by enabling simultaneous information processing and wireless power transfer [6]. While the former technique is based on transmitting wireless energy and information separately, the latter one aims at conveying both the energy and information in the same time slot. Nevertheless, in practical scenarios, it is difficult to perform information decoding and energy harvesting simultaneously. Accordingly, two practical system designs, namely time-switching (TS), and power-splitting (PS) were proposed in [6]. In the former protocol, the receiver switches over time between information decoding and EH, while in the latter, the received power is split into two streams, one for EH and the other for information processing [11].

This work was supported in part by Khalifa University under Grant No. KU/RC1-C2PS-T2/8474000137 and Grant No. KU/FSU-8474000122.

E. Illi and F. El Bouanani are with ENSIAS College of Engineering, Mohammed V University, Rabat 10000, Morocco (e-mails: {elmehdi.illi, f.elbouanani}@um5s.net.ma).

P. C. Sofotasios is with the Center for Cyber-Physical Systems, Department of Electrical Engineering and Computer Science, Khalifa University, PO Box 127788, Abu Dhabi, UAE and also with the Department of Electrical Engineering, Tampere University, 33014, Tampere, Finland (e-mail: p.sofotasios@ieee.org).

S. Muhaidat is with the Center for Cyber-Physical Systems, Department of Electrical Engineering and Computer Science, Khalifa University, Abu Dhabi 127788, UAE, and also with the Department of Systems and Computer Engineering, Carleton University, Ottawa, ON K1S 5B6, Canada (e-mail: muhaidat@ieee.org).

D. B. da Costa is with the Department of Computer Engineering, Federal University of Ceará (UFC), Sobral-CE, Brazil (e-mail: danielbcosta@ieee.org).

F. Ayoub is with CRMEF, Kenitra 14000, Morocco (e-mail: ayoub@crmefk.ma).

A. Al-Fuqaha is with the Information and Computing Technology Division, Hamad Bin Khalifa University and Computer Science Department, Western Michigan University (email: ala@ieee.org).

On the other hand, RF communications are often impaired due to multipath fading and shadowing random phenomena, caused by the presence of reflectors, scatterers, and obstacles [12]. Within this context, several existing distributions were introduced, supported by field test measurements, to accurately describe the statistics of the signal variations due to fading, namely Rayleigh for a non-line of sight (NLOS)-based link, Rician for a LOS-based communication, as well as Nakagami-m and Weibull distributions for urban outdoor environments. In [13], the α-μ model was proposed as a generalized distribution for modeling the fading amplitude in a mobile radio channel, since it includes a vast majority of the well-known fading distributions, namely Rayleigh, Weibull, and Nakagami-m, as special cases. Such a model represents the fading distribution in non-homogeneous and non-linear environments [13].

Multihop relaying, where information is communicated between two terminals (nodes) over multiple hops, has been extensively investigated in the literature. This multihop approach realizes several key advantages as compared to the single-hop scenario, e.g., lower power consumption and better throughput. A variant of multihop relaying, known as cooperative diversity, or cooperative communications [14]–[16], has emerged as a promising approach to increase spectral and power efficiencies, network coverage, and reduce outage probability, mostly used in infrastructure-less based networks. In cooperative communications, the relaying process signals overheard from the source terminal and re-transmit them toward a destination. Two common relaying techniques are the decode-and-forward (DF) and the amplify-and-forward (AF) [17]. In DF relaying, the relay terminal decodes a received signal and then re-encodes it (possibly using a different codebook) for transmission to a destination. With AF relaying, the relay terminal re-transmits a scaled version of the received signal without any attempt to decode it [17]. Also, in scenarios, the cooperating nodes are typically located at different locations, and, therefore, asymmetric channels are often experienced in practice [18]. Therefore, several research studies investigated the performance analysis of dual-hop transmission systems under asymmetric fading environments, for AF and DF relaying. Specifically, in [19], the authors investigated the performance of DF relaying systems in mixed fading environments, which were modeled by Rayleigh/Generalized-Gamma fading channels. The authors in [20] examined the performance of a dual-hop system in mixed fading environments subject to Rayleigh/Rician scenarios. In [21], the analysis was carried out assuming a dual-hop DF relaying protocol with HARQ retransmission scheme in Rayleigh/Rician environments, while the work in [18] dealt with the analysis of a full-duplex DF relaying system over generalized fading channels. Finally, the work in [22] focused on the analysis of a multiple-input multiple-output (MIMO) relay network with dual-hop AF relaying, over asymmetric fading channels.

Within the context of EH, the performance of multi-hop EH-based wireless communication systems has been widely investigated in the literature. As far as the WPC is concerned, the work in [23] inspects the throughput maximization of a dual-hop WPC-based system. The same authors in [24] analyzed a similar setup by inspecting the resource allocation in full-duplex (FD) WPC network. Likewise, a similar analysis on a dual-hop FD WPC network is investigated in [25]. From another front, in [26], the authors dealt with the bit error rate performance of a dual-hop SWIPT-based system, by considering the AF and DF protocols and taking into account TS and PS, over Nakagami-m fading channels. In [27], the performance of a dual-hop full-duplex SWIPT-based system is analyzed, by considering both AF and DF protocols, while [28] dealt with the analysis of a multi-hop cognitive-radio EH-based network. The works in [9] and [29] analyzed the performance of a dual-hop multi-relay communication scheme and a MIMO dual-hop SWIPT-based communication system, respectively. On the other hand, other works [30]–[32] analyzed the throughput, outage, or the physical layer security of SWIPT-based systems with asymmetric fading conditions.

Although the previous works added new insights, they have mainly focused on: outage probability, error rate, and ergodic capacity analysis. Furthermore, sporadic results have been reported on the performance of dual-hop EH-based communication systems, employing the SWIPT technique, subject to asymmetric fading conditions. To the best of the authors' knowledge, the performance analysis of asymmetric dual-hop EH-based communication systems with finite battery capacity, including the average symbol error rate (ASER) and the average channel capacity (ACC) over two distinct adaptive transmission policies, has not been addressed yet in the open literature. Owing to this fact, this work aims to fill this gap by investigating the ASER and capacity performance of EH-based dual-hop fixed-gain AF relaying systems over four different adaptive transmit policies, namely, optimal power adaptation (ORA), optimal power and rate adaptation (OPRA), channel inversion with fixed rate (CIFR), and truncated channel inversion with fixed rate (TCIFR). In particular, an AF relay node (R) equipped with a finite-capacity battery, and employing EH SWIPT technique, is used to forward the information signal from the source (S) to the destination (D). Furthermore, S can communicate directly with D. This latter employs a maximal-ratio combining (MRC) receiver to combine incoming signals from S and R. Importantly, asymmetric fading conditions are assumed for all the system's links, by considering the Nakagami-m model for representing the first hop link's fading and the α-μ fading model for both the second hop and the direct link (i.e., S-D). Moreover, both TS and PS SWIPT protocols are considered in the analysis. Pointedly, the main contributions of this paper can be summarized as follows:

- Novel generalized closed-form expressions are derived for the cumulative distribution function (CDF) of the end-to-end SNR of the considered system, for both TS and PS protocols.
- Based on the statistical properties of the total signal-to-noise ratio (SNR), novel closed-form expressions are derived for the ASER of various coherent modulation schemes and the ACC under four different adaptive policies. The obtained results highlight that the system's ASER remains below 10^{-5} when the transmit power-to-noise ratios at the relay and destination are more than

This article has been accepted for publication in a future issue of this journal, but has not been fully edited. Content may change prior to final publication. Citation information: DOI 10.1109/TGCN.2020.3035512, IEEE Transactions on Green Communications and Networking

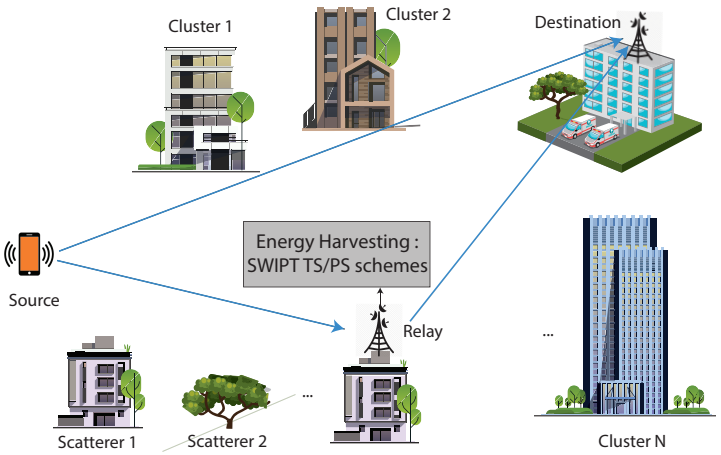

Fig. 1: System model.

30 dB. The results show also that the ACC under OPRA policy slightly outperforms its ORA counterpart in mid and high SNR regimes.

- Though the derived CDF expression is given in terms of the bivariate Fox's H-function (FH), the performance metrics were derived in terms of either univariate or bivariate FHs, by developing a benchmark for the computation of the Mellin transform of the bivariate FH.
- To gain additional insights into the performance of the system, the achievable diversity order has been derived.

The remainder of this paper is organized as follows: Section II describes the considered system and channel models, while Section III is dedicated to the derived CDF of the end-to-end SNR alongside some useful results for the system's performance analysis. Section IV focuses on the performance analysis of the considered system by retrieving the ASER and the capacity under four adaptive policies. Numerical results and discussions are presented in Section V, while conclusions are drawn in Section VI.

II. Channel and System Models

We consider a dual-hop EH-based wireless communication system with a fixed-gain AF relay, operating with both TS and PS protocols, as shown in Fig. 1 [1]. A source terminal S communicates with a destination D, either directly or through a fixed relay node R over two time slots. Under the TS protocol, S broadcasts the information signal towards R and D during the first part of the first time slot and transmits the energy signal to R during the remaining part of it. For PS, the power is divided at the relay into two portions, one for information decoding and the other for EH. Next, the relay R uses the harvested energy during Phase-1 to forward the information signal to D after amplifying it with a fixed gain. Subsequently, D combines the incoming signals from both paths (i.e., direct and dual-hop links) with the aid of the MRC receiver. We further assume asymmetric fading conditions over the S-R, R-D, and S-D links. In particular, the S-R link is subject to the Nakagami-m fading model, while the R-D and S-D channels undergo the α-μ distribution. Furthermore, the channel gains of all links are assumed to be statistically independent.

[1]Nakagami-m fading model has been widely advocated in literature for providing a good agreement with urban land-mobile communication scenarios, where scatterers are randomly distributed [12], [33]. On the other hand, α-μ model can generalize fading scenarios for non-homogeneous and non-linear environments, where the scatterers are grouped in clusters [13]. Also, this model includes the Nakagami-m fading model as a special case.

A. Phase I: S-R hop

1) Information Signal Transmission:

- **TS protocol**: The source node sends during the first $(1-\varepsilon)T_0$ seconds the information signal x_s to R as well as to D through a direct link, where ε stands for the time portion dedicated to the EH, and T_0 is the time slot dedicated to the S-R communication. The received instantaneous SNR at R and D can be expressed as [12]

$$\gamma_{SX}^{(TS)} = \frac{P_S}{d_{SX}^{\delta} N_X} |h_{SX}|^2 ; X \in \{R, D\}, \quad (1)$$

respectively, in which P_S denotes the transmit power, d_{AB} is the A-B distance with $A, B \in \{S, R, D\}$ and $A \neq B$, δ is the path-loss exponent, h_{AB} denotes the A-B channel fading coefficient with average fading power $\Omega_{AB} = \mathbb{E}_{|h_{AB}|}\left[|h_{AB}|^2\right]$, $\mathbb{E}_Z[.]$ denotes the expected value with respect to the random variable Z, and N_X denotes the additive white Gaussian noise (AWGN) power at node X.

- **PS protocol:** S sends during the first time slot T_0 the information signal x with power P_S. The relay splits the power of the received signal into two parts: A portion $1-\varrho$ of the received power at the relay is dedicated to information decoding, where $0 < \varrho < 1$ is the power portion dedicated to EH. The received instantaneous SNR at R and D, assuming PS protocol is formulated as

$$\gamma_{SX}^{(PS)} = \frac{(1-\varrho) P_S}{d_{SX}^{\delta} N_X} |h_{SX}|^2 ; X \in \{R, D\}, \quad (2)$$

Consequently, the instantaneous SNR at node X can be expressed for both SWIPT protocols as follows

$$\gamma_{SX} = \frac{(1-\varsigma) P_S}{d_{SX}^{\delta} N_X} |h_{SX}|^2 , \quad (3)$$

with ς equal to either 0 for TS, and ϱ for PS, where their respective average values are given as $\overline{\gamma}_{SX} = \frac{(1-\varsigma)P_S}{d_{SX}^{\delta} N_X} \Omega_{SX}$.

2) Energy Harvesting: For the TS protocol, the information is transmitted from S to D via R during a total time of T_0. Under this scheme, ε represents the portion of T_0 in which the relay harvests energy from the source signal, where $0 < \varepsilon < 1$. Subsequently, data transmission is carried out in the remaining block transmission time. However, for the PS protocol, a portion ϱ of the received power at the receiver is harvested by the relay. As a result, the collected energy by the relay for both protocols can be written as [9]

$$E_R = \frac{\theta \kappa T_0 P_S |h_{SR}|^2}{d_{SR}^{\delta}}, \quad (4)$$

where κ denotes ε for TS and ϱ for PS, while θ stands for the conversion efficiency of the relay's energy harvester.

The relay R uses the harvested energy to amplify the received signal and to transmit it to D during the time slot T_1. Henceforth, a finite battery storage model is assumed, where the harvested energy at the relay, E_R, can either be less than the relay battery capacity or exceeds it. In the former case, the relay node communicates with D with a power $P_E = \frac{E_R}{T_1}$, while in the latter one, the R-D communication is ensured with the whole available power at the battery; i.e., $P_B = \frac{B_R}{T_1}$, with B_R being the battery capacity in mAh×V. Thus, the relay transmit power P_R can be expressed as

$$P_R = \begin{cases} P_E, & E_R < B_R \\ P_B, & E_R \geq B_R \end{cases}. \tag{5}$$

B. Phase II: R-D hop

In this part, two cases can be distinguished, namely $E_R < B_R$ and $E_R \geq B_R$. Furthermore, $\gamma_{RD}^{(1)}$ and $\gamma_{RD}^{(2)}$ denote the second hop's SNR corresponding to these two cases, respectively.

1) $E_R < B_R$: During the second time slot T_1, the relay amplifies the signal received from S by a fixed gain and forwards it to D using the harvested power P_E.

The received SNR at D over the R-D link, when $E_R < B_R$, is given by

$$\begin{aligned} \gamma_{RD}^{(1)} &= \frac{P_E \left|h_{RD}\right|^2}{d_{RD}^{\delta} N_D} \\ &= P_E \Upsilon_{RD}, \end{aligned} \tag{6}$$

with an average value $\overline{\gamma}_{RD}^{(1)} = \mathbb{E}_{P_E}\left[P_E\right] \overline{\Upsilon}_{RD}$, where $\mathbb{E}_{P_E}\left[P_E\right] = \frac{\theta \kappa T_0 P_s \Omega_{SR}}{T_1 d_{SR}^{\delta}}$ and $\overline{\Upsilon}_{RD} = \frac{\Omega_{RD}}{d_{RD}^{\delta} N_D}$.

2) $E_R \geq B_R$: In this scenario, the relay R forwards the information signal to D, after amplifying it with a fixed gain with power $P_B = \frac{B_R}{T_1}$. Consequently, the received SNR at D is expressed as

$$\gamma_{RD}^{(2)} = P_B \Upsilon_{RD}, \tag{7}$$

with an average value $\overline{\gamma}_{RD}^{(2)} = P_B \overline{\Upsilon}_{RD}$. At the end of the two time slots, the destination D combines through MRC technique the received SNRs from the dual-hop path (i.e., S-R-D) and from the direct one (i.e., S-D) as follows

$$\gamma_T = \gamma_{eq} + \gamma_{SD}, \tag{8}$$

where γ_{eq} is the received SNR at D through the dual-hop link, expressed for the case of a fixed-gain AF relaying as [17]

$$\gamma_{eq} = \frac{\gamma_{SR}\gamma_{RD}}{\gamma_{RD} + C}, \tag{9}$$

with C being a fixed-gain relaying constant.

In this work, Nakagami-m distribution is considered for modeling the fading amplitude of the S-R hop. As a consequence, the received SNR at the relay is Gamma-distributed with PDF and CDF expressions given as [12]

$$f_{\gamma_{SR}}(z) = \left(\frac{m_{SR}}{\overline{\gamma}_{SR}}\right)^{m_{SR}} \frac{z^{m_{SR}-1}}{\Gamma(m_{SR})} \exp\left(-\frac{m_{SR}}{\overline{\gamma}_{SR}} z\right), \tag{10}$$

$$F_{\gamma_{SR}}(z) = \frac{\gamma_{\text{inc}}\left(m_{SR}, \frac{m_{SR}}{\overline{\gamma}_{SR}} z\right)}{\Gamma(m_{SR})}, \tag{11}$$

respectively, where m_{SR} stands for the Nakagami-m fading parameter, $\Gamma(.)$ and $\gamma_{\text{inc}}(.,.)$ denote the Gamma and the lower-incomplete Gamma functions, respectively [34, Eqs. (8.310.1), (8.350.1)]. In a similar way, it can be easily shown that P_E in (5) is also Gamma-distributed with PDF and CDF given as

$$f_{P_E}(z) = \Psi^{m_{SR}} \frac{z^{m_{SR}-1}}{\Gamma(m_{SR})} \exp(-\Psi z), \tag{12}$$

and

$$F_{P_E}(z) = \frac{\gamma_{\text{inc}}(m_{SR}, \Psi z)}{\Gamma(m_{SR})}, \tag{13}$$

respectively, where $\Psi = \frac{m_{SR} T_1 d_{SR}^{\delta}}{\theta \kappa T_0 P_s \Omega_{SR}}$. On the other hand, α-μ fading is considered for the R-D and S-D links, with PDFs given as [13]

$$\begin{aligned} f_{\Upsilon_{RD}}(z) = &\frac{\alpha_{RD} \mu_{RD}^{\mu_{RD}}}{2\Gamma(\mu_{RD}) \overline{\Upsilon}_{RD}} \left(\frac{z}{\overline{\Upsilon}_{RD}}\right)^{\frac{\alpha_{RD}\mu_{RD}}{2}-1} \\ &\times e^{-\mu_{RD}\left(\frac{z}{\overline{\Upsilon}_{RD}}\right)^{\frac{\alpha_{RD}}{2}}}, \end{aligned} \tag{14}$$

$$\begin{aligned} f_{\gamma_{SD}}(z) = &\frac{\alpha_{SD} \mu_{SD}^{\mu_{SD}}}{2\Gamma(\mu_{SD}) \overline{\gamma}_{SD}} \left(\frac{z}{\overline{\gamma}_{SD}}\right)^{\frac{\alpha_{SD}\mu_{SD}}{2}-1} \\ &\times e^{-\mu_{SD}\left(\frac{z}{\overline{\gamma}_{SD}}\right)^{\frac{\alpha_{SD}}{2}}}, \end{aligned} \tag{15}$$

with $\overline{\gamma}_{SD} = \frac{P_S \Omega_{SD}}{d_{SD}^{\delta} N_D}$, where α_{XD} and μ_{XD} $(X \in \{S, R\})$ denote the two physical fading parameters reflecting the environment non-linearity and the number of multipath clusters, respectively. Thus, the respective CDFs of Υ_{RD} and γ_{SD} are given as

$$F_{\Upsilon_{RD}}(z) = \frac{\gamma_{\text{inc}}\left(\mu_{RD}, \mu_{RD}\left(\frac{z}{\overline{\Upsilon}_{RD}}\right)^{\frac{\alpha_{RD}}{2}}\right)}{\Gamma(\mu_{RD})}, \tag{16}$$

and

$$F_{\gamma_{SD}}(z) = \frac{\gamma_{\text{inc}}\left(\mu_{SD}, \mu_{SD}\left(\frac{z}{\overline{\gamma}_{SD}}\right)^{\frac{\alpha_{SD}}{2}}\right)}{\Gamma(\mu_{SD})}, \tag{17}$$

respectively.

III. Statistical properties

In this section, the CDF expression in closed-form for the total SNR is derived.

A. Cumulative Distribution Function

Proposition 1. *The CDF expression of the total combined SNR at D can be expressed as*

$$F_{\gamma_T}(z) = F_{\gamma_{SD}}(z) - \frac{F_{P_E}(P_B)}{\Gamma(m_{SR})} T_1(z) - F_{P_E}^{c}(P_B)\, T_2(z), \tag{18}$$

where $F_X^c(.)$ is the complementary CDF of X, and $T_i(z)$ $(i = 1, 2)$ is given in (19) at the top of the next page, with $\eta_i = \mu_{RD}\left(\frac{m_{SR}^{3-i} C}{\overline{\gamma}_{SR}\overline{\gamma}_{RD}^{(i)}}\right)^{\frac{\alpha_{RD}}{2}}$, $\vartheta = \mu_{SD}\left(\frac{1}{\overline{\gamma}_{SD}}\right)^{\frac{\alpha_{SD}}{2}}$, $h_{n,p,k} = n - p + k$, $\mathcal{E}_1 = \left(-h_{n,p,k}, \frac{\alpha_{RD}}{2}, \frac{\alpha_{SD}}{2}\right)$, $\mathcal{E}_2 = \left(-h_{n,p,k}, \frac{\alpha_{RD}}{2}\right)$, $\Delta_1 = \left\{(\mu_{RD}, 1), \left(p, \frac{\alpha_{RD}}{2}\right), \left(m_{SR}, \frac{\alpha_{RD}}{2}\right)\right\}$,

This article has been accepted for publication in a future issue of this journal, but has not been fully edited. Content may change prior to final publication. Citation information: DOI 10.1109/TGCN.2020.3035512, IEEE Transactions on Green Communications and Networking

$$T_i(z)=\frac{\alpha_{RD}\alpha_{SD}}{4\Gamma(\mu_{SD})\Gamma(\mu_{RD})}\sum_{n=0}^{m_{SR}-1}\sum_{p=0}^{n}\sum_{k=0}^{\infty}\frac{(-1)^k\left(\frac{m_{SR}z}{\overline{\gamma}_{SR}}\right)^{h_{n,p,k}}}{p!\,(n-p)!k!}H_{0,1;1,4-i;1,1}^{0,0;4-i,1;1,1}\left(\eta_i z^{\frac{\alpha_{RD}}{2}},\vartheta z^{\frac{\alpha_{SD}}{2}}\left|\begin{array}{c}-;-:\mathcal{E}_2;-:\left(1,\frac{\alpha_{RD}}{2}\right);-\\-;\mathcal{E}_1:\Delta_i;-:(\mu_{SD},1);-\end{array}\right.\right). \tag{19}$$

$\Delta_2=\left\{(\mu_{RD},1),\left(p,\frac{\alpha_{RD}}{2}\right)\right\}$, *and* $H_{p_1,q_1;p_2,q_2;p_3,q_3}^{0,n_1;m_2,n_2;m_3,n_3}\left(x,y\,|.\right)$ *denotes the bivariate FH [35].*

Proof: The proof is provided in Appendix A. ∎

Remark 1. *One can note evidently that the CDF of the total SNR at the receiver, given in (18), is composed of three terms. To this end, when the relay battery capacity is sufficiently higher and the source transmit power is lower, the probability* $F_{P_E}\left(P_B\right)$ *tends to* 1 $\left(i.e.,\ F_{P_E}^{c}\left(P_B\right)\to 0\right)$. *Therefore, the CDF of* γ_T *depends mainly, in this case, on the first two terms, which corresponds to the CDF expression with an infinite battery capacity assumption. Analogously, for lower relay battery capacity and higher source transmit power,* $F_{P_E}\left(P_B\right)\to 0$. *As a result, the second term in the CDF tends to zero, and the relay transmits to D with constant power (i.e.,* P_B *is constant).*

Corollary 1. *The achievable system's diversity order in high SNR regime* $\left(i.e.,\ \overline{\gamma}_{SR},\overline{\gamma}_{RD}^{(i)},\overline{\gamma}_{SD}\to\infty\right)$ *is given as*

$$G_d=\frac{\alpha_{SD}\mu_{SD}}{2}+m_{SR}+\min\left(m_{SR},\frac{\alpha_{RD}\mu_{RD}}{2}\right). \tag{20}$$

Proof: The proof is provided in Appendix B. ∎

Remark 2. *One can note from (20) that the system's achievable diversity order depends exclusively on the severity fading parameters of all links. Particularly, it is evident from the aforementioned equation that such a diversity order depends only on the direct and first dual-hop links for enhanced second hop link's conditions.*

Lemma 1. *The moment of order* $n=-1$ *of* γ_T *can be expressed as follows*

$$\mathbb{E}_{\gamma_T}\left[\gamma_T^{-1}\right]=\mathcal{K}_{SD}-\frac{F_{P_E}\left(P_B\right)}{\Gamma(m_{SR})}\mathcal{Y}_1-F_{P_E}^{c}\left(P_B\right)\mathcal{Y}_2, \tag{21}$$

where

$$\mathcal{K}_{\mathcal{SD}}=\frac{\mu_{SD}^{\frac{2}{\alpha_{SD}}}\Gamma\left(\mu_{SD}-\frac{2}{\alpha_{SD}}\right)}{\Gamma(\mu_{SD})\overline{\gamma}_{SD}}, \tag{22}$$

and

$$\begin{aligned}\mathcal{Y}_i=&\frac{\mu_{RD}^{\frac{2}{\alpha_{RD}}}m_{SR}^{3-i}C\alpha_{SD}}{2\Gamma(\mu_{SD})\Gamma(\mu_{RD})\overline{\gamma}_{SR}\overline{\gamma}_{RD}^{(i)}}\sum_{n=0}^{m_{SR}-1}\sum_{p=0}^{n}\frac{1}{p!\,(n-p)!}\\&\times\sum_{k=0}^{\infty}\frac{(-1)^k}{k!}\left(\frac{\overline{\gamma}_{RD}^{(i)}}{m_{SR}^{2-i}C\mu_{RD}^{\frac{2}{\alpha_{RD}}}}\right)^{h_{n,p,k}}\\&\times H_{5,1}^{1,4}\left(\left[\frac{\mu_{SD}^{\frac{2}{\alpha_{SD}}}\overline{\gamma}_{SR}\overline{\gamma}_{RD}^{(i)}}{\mu_{RD}^{\frac{2}{\alpha_{RD}}}m_{SR}^{3-i}C\overline{\gamma}_{SD}}\right]^{\frac{\alpha_{SD}}{2}}\middle|\,\Psi\right),i=1,2,\end{aligned} \tag{23}$$

with $\Psi=\left(\begin{array}{c}\mathcal{Q}_1,\mathcal{Q}_2,\mathcal{Q}_3,\left(1,\frac{\alpha_{SD}}{2}\right);\left(2,\frac{\alpha_{SD}}{2}\right)\\(\mu_{RD},1);-\end{array}\right)$,
$\mathcal{Q}_1=\left(1-\mu_{RD}-\frac{2}{\alpha_{RD}}\left(h_{n,p,k}-1\right),\frac{\alpha_{SD}}{\alpha_{RD}}\right)$,
$\mathcal{Q}_2=\left(2-n-k,\frac{\alpha_{SD}}{2}\right)$, *and* $\mathcal{Q}_3=\left(2-m_{SR}-h_{n,p,k},\frac{\alpha_{SD}}{2}\right)$.

Proof: The proof is provided in Appendix C. ∎

Corollary 2. *The integral* $\mathcal{I}(x)=\int_x^{\infty}\frac{f_{\gamma_T}(z)}{z}dz$ *can be expressed as*

$$\mathcal{I}(x)=\mathcal{L}_{SD}\left(x\right)-\frac{F_{P_E}\left(P_B\right)}{\Gamma(m_{SR})}\mathcal{Z}_1\left(x\right)-F_{P_E}^{c}\left(P_B\right)\mathcal{Z}_2\left(x\right)-\frac{F_{\gamma_T}(x)}{x}. \tag{24}$$

with

$$\mathcal{L}_{SD}\left(x\right)=\mathcal{K}_{SD}-\mathcal{M}_{SD}\left(x\right), \tag{25}$$

$$\mathcal{Z}_i\left(x\right)=\mathcal{Y}_i-\mathcal{W}_i\left(x\right);i=1,2, \tag{26}$$

$$\mathcal{M}_{SD}(x)=\frac{2}{\alpha_{SD}\Gamma(\mu_{SD})x}G_{2,3}^{1,2}\left(\vartheta x^{\frac{\alpha_{SD}}{2}}\left|\begin{array}{c}1+\frac{2}{\alpha_{SD}},1;-\\\mu_{SD};0,\frac{2}{\alpha_{SD}}\end{array}\right.\right), \tag{27}$$

and

$$\begin{aligned}\mathcal{W}_i\left(x\right)=&\frac{\alpha_{RD}\alpha_{SD}}{4\Gamma(\mu_{SD})\Gamma(m_{SR})\Gamma(\mu_{RD})x}\sum_{n=0}^{m_{SR}-1}\sum_{p=0}^{n}\sum_{k=0}^{\infty}\frac{(-1)^k}{p!\,(n-p)!k!}\\&\times\left(\frac{m_{SR}x}{\overline{\gamma}_{SR}}\right)^{h_{n,p,k}}H_{1,2;1,4-i;1,1}^{0,1;4-i,1;1,1}\left(\eta_i x^{\frac{\alpha_{RD}}{2}},\vartheta x^{\frac{\alpha_{SD}}{2}}\middle|\,\Phi_i\right),\end{aligned} \tag{28}$$

for $i\leq 2$, *and*
$\Phi_i=\left(\begin{array}{c}\left(3-h_{n,p,k},\frac{\alpha_{RD}}{2},\frac{\alpha_{SD}}{2}\right);-:\mathcal{E}_2;-:\left(1,\frac{\alpha_{SD}}{2}\right);-\\-;\mathcal{E}_1,\left(2-h_{n,p,k},\frac{\alpha_{RD}}{2},\frac{\alpha_{SD}}{2}\right):\Delta_i;-:(\mu_{SD},1);-\end{array}\right)$.

Proof: The proof is provided in Appendix D. ∎

Remark 3. *It is worth mentioning that the use of the transforms given in* ***Lemma 1*** *and* ***Corollary 2*** *are key in the performance analysis process, as no closed-form expressions can be derived without them. Specifically, such results represent the Mellin transform of the bivariate FH. To the best of our knowledge, such transforms do not exist in explicit form in the open literature. Promisingly, the original forms have been moved from triple integrals (over double complex integration contours* (C_s,C_t) *and a single real integration interval over* z*), to either simple (univariate FH), or double (bivariate FH) integrals. Therefore, such results can assist readers in deriving similar performance metrics when the statistical properties are expressed in terms of the bivariate FH.*

IV. Performance Evaluation

In this section, closed-form expressions of the ASER for different modulation techniques, and the ACC under four different adaptive transmission policies, namely ORA, OPRA, CIFR, and TCIFR, are derived.

This article has been accepted for publication in a future issue of this journal, but has not been fully edited. Content may change prior to final publication. Citation information: DOI 10.1109/TGCN.2020.3035512, IEEE Transactions on Green Communications and Networking

A. Average Symbol Error Rate

The ASER is a common performance metric for evaluating the communication's reliability over fading channels. For a communication system subject to random fading, it is defined as the statistical average value of the instantaneous symbol error rate. The ASER is defined as

$$\overline{P}_{se} = \int_0^\infty P_{se}(z) f_{\gamma_T}(z) dz, \tag{29}$$

which for various modulation schemes, it is given by

$$\overline{P}_{se} = \rho \int_0^\infty \operatorname{erfc}\left(\sqrt{\tau z}\right) f_{\gamma_T}(z) dz, \tag{30}$$

where ρ and τ are two modulation-dependant parameters [36], and $\operatorname{erfc}(.)$ stands for the complementary error function [34, Eqs. (8.250.1, 8.250.4)].

Proposition 2. *The ASER of the considered communication system for a variety of modulation schemes can be expressed as*

$$\overline{P}_{se} = \frac{\rho}{\sqrt{\pi}} \left(\mathcal{H}_{SD} - \frac{F_{P_E}(P_B)}{\Gamma(m_{SR})} \mathcal{V}_1 - F^c_{P_E}(P_B)\, \mathcal{V}_2 \right), \tag{31}$$

$$\mathcal{H}_{SD} = \frac{1}{\Gamma(\mu_{SD})} H^{1,2}_{2,2}\left(\frac{\vartheta}{\tau^{\frac{\alpha_{SD}}{2}}} \,\middle|\, \begin{matrix} \left(\frac{1}{2}, \frac{\alpha_{SD}}{2}\right), (1,1) \,;- \\ (\mu_{SD}, 1)\,; (0,1) \end{matrix} \right), \tag{32}$$

and $\mathcal{V}_i$ is given in (33) at the top of the next page for $i = 1, 2$, with $\mathcal{E}_3 = \left(\frac{1}{2} - h_{n,p,k}, \frac{\alpha_{RD}}{2}, \frac{\alpha_{SD}}{2}\right)$, and $H^{m,n}_{p,q}(.|.)$, $q \geq m$, $p \geq n$, is the FH [37, Eqs. (1.1.1, 1.1.2)].

Proof: The proof is provided in Appendix E. ∎

It is noteworthy that the bivariate FH can be implemented efficiently in most popular computer software, such as Matlab or Mathematica [36]. Such a function can be implemented either through a double numerical integration over two complex contours or with the aid of the residues theorem applied on the poles of Gamma functions in (33) [37, Theorem (1.2)], when the left half-plane poles are separated from the right half-plane ones.

B. Optimal rate adaptation policy

The bandwidth-normalized ACC under constant transmission power, namely ORA adaptive policy, is often known as Shannon capacity. By definition, it is expressed as [12]

$$\overline{C}_{ORA} = \int_0^\infty \log_2(1+z)\, f_{\gamma_T}(z) dz, \tag{34}$$

or it can be alternatively expressed in terms of the complementary CDF of the SNR as

$$\overline{C}_{ORA} = \frac{1}{\log(2)} \int_0^\infty \frac{F^c_{\gamma_T}(z)}{1+z} dz. \tag{35}$$

Proposition 3. *The ACC under ORA policy of the considered AF dual-hop system is expressed as*

$$\overline{C}_{ORA} = \frac{1}{\log(2)} \left[\mathcal{G}_{SD} + \frac{F_{P_E}(P_B)}{\Gamma(m_{SR})} \mathcal{X}_1 + F^c_{P_E}(P_B)\, \mathcal{X}_2 \right], \tag{36}$$

where

$$\mathcal{G}_{SD} = \frac{1}{\Gamma(\mu_{SD})} H^{3,1}_{2,3}\left(\vartheta \,\middle|\, \begin{matrix} (0, \frac{\alpha_{SD}}{2}); (1,1) \\ (0,1), (\mu_{SD}, 1), (0, \frac{\alpha_{SD}}{2}); - \end{matrix} \right), \tag{37}$$

$$\mathcal{X}_i = \frac{\alpha_{RD}\alpha_{SD}}{4\Gamma(\mu_{SD})\Gamma(\mu_{RD})} \sum_{n=0}^{m_{SR}-1} \sum_{p=0}^{n} \frac{1}{p!\,(n-p)!} \sum_{k=0}^{\infty} \frac{(-1)^k}{k!} \times \left(\frac{m_{SR}}{\overline{\gamma}_{SR}} \right)^{h_{n,p,k}} H^{0,1;4-i,1;1,1}_{1,0;1,4-i;1,1}\left(\eta_i, \vartheta \middle| \Xi_i \right), i = 1, 2, \tag{38}$$

with $\Xi_i = \left(\begin{matrix} \left(1 + h_{n,p,k}, -\frac{\alpha_{RD}}{2}, -\frac{\alpha_{SD}}{2}\right); - : \mathcal{E}_2; - : \left(1, \frac{\alpha_{SD}}{2}\right); - \\ -; - : \Delta_i; - : (\mu_{SD}, 1); - \end{matrix} \right)$.

Proof: The proof is provided in Appendix F. ∎

C. Optimal power and rate adaptation policy

The bandwidth-normalized ACC under OPRA policy is defined as the capacity of a fading channel with the source transmit power is adapted to maximize the achievable end-to-end capacity. Mathematically, it is expressed as [38]

$$\overline{C}_{OPRA} = \int_{\gamma^*}^\infty \log_2\left(\frac{z}{\gamma^*}\right) f_{\gamma_T}(z) dz, \tag{39}$$

where γ^* is the optimal cutoff SNR, below which no transmission is performed, satisfying the following equation

$$\int_{\gamma^*}^\infty \left(\frac{1}{\gamma^*} - \frac{1}{z} \right) f_{\gamma_T}(z) dz - 1 = 0. \tag{40}$$

Proposition 4. *The ACC under OPRA policy of the considered AF dual-hop system is expressed as*

$$\overline{C}_{OPRA} = \frac{\mathcal{O}_{SD}(\gamma^*) + \frac{F_{P_E}(P_B)}{\Gamma(m_{SR})} \mathcal{N}_1(\gamma^*) + F^c_{P_E}(P_B)\, \mathcal{N}_2(\gamma^*)}{\log(2)}, \tag{41}$$

where

$$\mathcal{O}_{SD}(\gamma^*) = \frac{H^{3,0}_{2,3}\left(\vartheta (\gamma^*)^{\frac{\alpha_{SD}}{2}} \,\middle|\, \begin{matrix} -; (1,1), \left(1, \frac{\alpha_{SD}}{2}\right) \\ (\mu_{SD}, 1), (0,1), \left(0, \frac{\alpha_{SD}}{2}\right); - \end{matrix} \right)}{\Gamma(\mu_{SD})}, \tag{42}$$

and $\mathcal{N}_i(\gamma^*)$ is given in (43) at the top of the next page for $i \leq 2$, with $\Lambda_{n,p,k} = \left\{ \left(1 + h_{n,p,k}, -\frac{\alpha_{RD}}{2}, -\frac{\alpha_{SD}}{2}\right); \left(1 - h_{n,p,k}, \frac{\alpha_{RD}}{2}, \frac{\alpha_{SD}}{2}\right) \right\}$, and γ^* is the unique solution of the following equation [39]

$$\frac{F^c_{\gamma_T}(x)}{x} - \mathcal{I}(x) - 1 = 0. \tag{44}$$

Proof: The proof is provided in Appendix G. ∎

D. Channel inversion with fixed rate Policy

The CIFR policy is an adaptive transmission policy which requires that the transmitter exploits the channel state information of all links (i.e., S-R and R-D, and S-D), so that a constant SNR is maintained at the receiver (i.e., it inverts

This article has been accepted for publication in a future issue of this journal, but has not been fully edited. Content may change prior to final publication. Citation information: DOI 10.1109/TGCN.2020.3035512, IEEE Transactions on Green Communications and Networking

$$\mathcal{V}_i = \frac{\rho\alpha_{RD}\alpha_{SD}}{4\sqrt{\pi}\Gamma(\mu_{SD})\Gamma(\mu_{RD})} \sum_{n=0}^{m_{SR}-1}\sum_{p=0}^{n}\sum_{k=0}^{\infty} \frac{(-1)^k \left(\frac{m_{SR}}{\overline{\gamma}_{SR}\tau}\right)^{h_{n,p,k}}}{p!\,(n-p)!k!} H_{1,1;1,4-i;1,1}^{0,1;4-i,1;1,1}\left(\frac{\eta_i}{\tau^{\frac{\alpha_{RD}}{2}}}, \frac{\vartheta}{\tau^{\frac{\alpha_{SD}}{2}}} \,\middle|\, \begin{matrix} \mathcal{E}_3;-:\mathcal{E}_2;-:\left(1,\frac{\alpha_{SD}}{2}\right);- \\ -;\mathcal{E}_1:\Delta_i;-:(\mu_{SD},1);- \end{matrix}\right). \tag{33}$$

$$N_i(\gamma^*) = \frac{\alpha_{RD}\alpha_{SD}}{4\Gamma(\mu_{SD})\Gamma(\mu_{RD})} \sum_{n=0}^{m_{SR}-1}\sum_{p=0}^{n}\sum_{k=0}^{\infty} \frac{(-1)^k \left(\frac{m_{SR}\gamma^*}{\overline{\gamma}_{SR}}\right)^{h_{n,p,k}}}{p!\,(n-p)!k!} \times H_{2,1;1,4-i;1,1}^{0,1;4-i,1;1,1}\left(\eta_i(\gamma^*)^{\frac{\alpha_{RD}}{2}}, \vartheta(\gamma^*)^{\frac{\alpha_{SD}}{2}} \,\middle|\, \begin{matrix} \Lambda_{n,p,k}:\mathcal{E}_2;-:\left(1,\frac{\alpha_{SD}}{2}\right);- \\ -;\mathcal{E}_1:\Delta_i;-:(\mu_{SD},1);- \end{matrix}\right). \tag{43}$$

the channel fading). Mathematically speaking, the bandwidth-normalized ACC under CIFR policy can be formulated as [39]

$$\overline{C}_{CIFR} = \log_2\left(1 + \left(\mathbb{E}_{\gamma_T}\left[\,\gamma_T^{-1}\right]\right)^{-1}\right). \tag{45}$$

Proposition 5. *The ACC under CIFR policy of the considered system is provided as*

$$\overline{C}_{CIFR} = \log_2\left(1 + \frac{1}{\mathcal{K}_{SD} - \frac{F_{P_E}(P_B)\mathcal{Y}_1}{\Gamma(m_{SR})} - F_{P_E}^c(P_B)\,\mathcal{Y}_2}\right). \tag{46}$$

Proof: By substituting (21), given in ***Lemma 1,*** *into (45), (46) is obtained.* ■

E. Truncated channel inversion with fixed rate policy

As in the above-mentioned CIFR policy, TCIFR policy consists of channel fading inversion, but only above a fixed cutoff SNR γ_0. The ACC under this policy is defined as

$$\overline{C}_{TCIFR} = \log_2\left(1 + \left[\int_{\gamma_0}^{\infty} \frac{f_{\gamma_T}(z)}{z} dz\right]^{-1}\right) F_{\gamma_T}^c(\gamma_0). \tag{47}$$

Proposition 6. *The ACC under TCIFR policy of the considered system is provided as*

$$\overline{C}_{TCIFR} = F_{\gamma_T}^c(\gamma_0)\log_2\left(1 + \left[\mathcal{I}(\gamma_0)\right]^{-1}\right). \tag{48}$$

Proof: Thus, by involving (24), given in ***Corollary 2****, into (47) with $x = \gamma_0$, (48) is attained.* ■

Remark 4. *Similarly to the CDF result, the expressions (31), (36), (41) as well as $\mathcal{I}(0)$ and $\mathcal{I}(\gamma_0)$ in (46) and (48) are composed of three or fours terms. Thus, the greater the battery capacity and the lower the source transmit power are, the greater $F_{P_E}(P_B)$ is $\left(i.e.,\ F_{P_E}^c(P_B) \to 0\right)$. Therefore, the third term in the derived metrics vanishes, which corresponds to an infinite battery capacity case. In contrast, the lower the relay battery size and the higher the source transmit power are, the smaller is $F_{P_E}(P_B)$ $(i.e.,\ F_{P_E}(P_B) \to 0)$. Consequently, the second term in the aforementioned expressions vanishes, and then R transmits to D with a constant harvested power.*

V. Numerical Results

In this section, some illustrative numerical examples are depicted in order to highlight the effects of the key system parameters on the obtained performance metrics. Without loss of generality, we set $m_{SR} = 3$ (except Fig. 11), $P_S = 100$ W (except Fig. 11), $\delta = 2$, $\Omega_{SR} = \Omega_{RD} = 5$, $\Omega_{SD} = 6$, $\mu_{RD} = 4.2$ (except Figs. 7 and 11), $\alpha_{RD} = 2.5$ (except Fig. 11), $\mu_{SD} = 3.5$ (except Fig. 11), $\alpha_{SD} = 3$ (except Fig. 11), $d_{SR} = 10$ m (except Figs. 2, 5, and 9), $d_{RD} = 25$m, $d_{SD} = 40$ m, $(\rho, \tau) = (0.5, 1)$ (except Fig. 3), $\frac{P_S}{N_D} = 25$ dB (except Figs. 4 and 6 and 11). In addition, the relaying fixed-gain constant was set to $C = 1$, $T_0 = T_1 = 1$ s, and $\varepsilon = \varrho = 0.7$ (except Figs. 5 and 7), $\theta = 0.7$, and $B_R = 500$ mAh×V. Additionally, the complex contours of integration in (31), (36), (41), (46), and (48) were chosen for both integrand terms on s and t, such that $\mathcal{C}_s =]c_s - j\infty, c_s + j\infty[$ and $\mathcal{C}_t =]c_t - j\infty, c_t + j\infty[$, with c_s and c_t are given in Table I.

Fig. 2 depicts the analytical and simulated ASER for BPSK modulation vs $\frac{P_S}{N_R}$ and the distance d_{SR} for the TS scheme, evaluated based on (29) and (31), respectively. The analytical and simulation results match, which demonstrates the accuracy of the derived results. Additionally, it can be clearly seen that the ASER decreases significantly with respect to $\frac{P_S}{N_R}$. In fact, the greater the transmit power, the higher is the harvested energy, and consequently, the better is the bit error rate performance. That is, for $\frac{P_S}{N_R} \to \infty$, the performance converges to that of an AWGN channel (no fading). Furthermore, one can remark also from Fig. 2 the nodes distance effect on the ASER performance. The farther S and R are, the more severe the path loss is, degrading the overall system's performance.

Fig. 3 shows the ASER vs $\frac{P_S}{N_R}$ for various modulation schemes, namely BPSK $(\rho = 0.5, \tau = 1)$, QPSK $(\rho = 1, \tau = 0.5)$, and BFSK $(\rho = 0.5, \tau = 0.5)$. One can notice that BPSK modulation scheme results in a better error rate performance compared to its BFSK and QPSK counterparts. Furthermore, the ASER curves present a steady behavior, particularly at low $\frac{P_S}{N_R}$ values (less than 20 dB). In fact, in this

This article has been accepted for publication in a future issue of this journal, but has not been fully edited. Content may change prior to final publication. Citation information: DOI 10.1109/TGCN.2020.3035512, IEEE Transactions on Green Communications and Networking

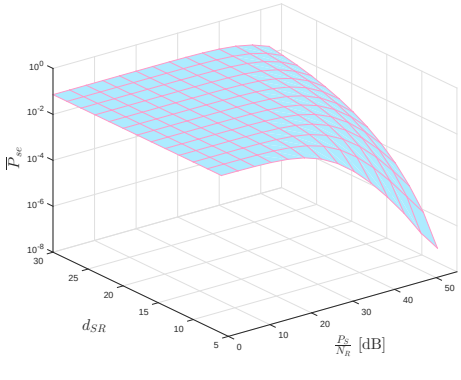

Fig. 2. ASER vs $\frac{P_S}{N_R}$ and d_{SR} for TS.

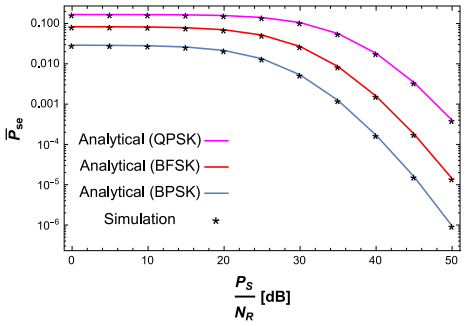

Fig. 3. ASER vs $\frac{P_S}{N_R}$ for various modulations.

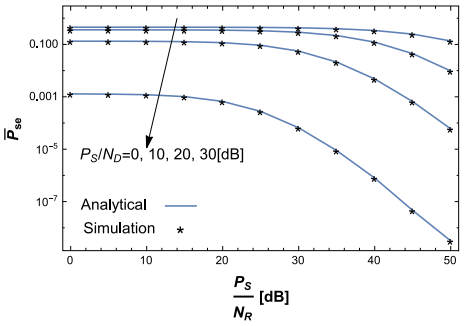

Fig. 4. ASER vs $\frac{P_S}{N_R}$ for several $\frac{P_S}{N_D}$ values.

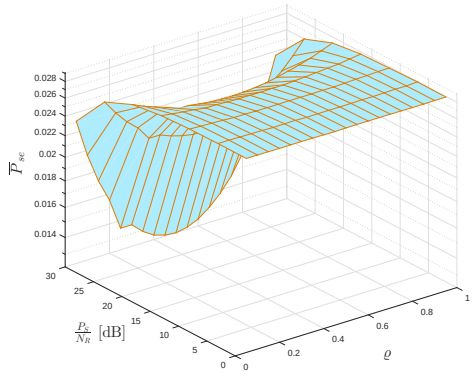

Fig. 5. ASER for PS vs ϱ and $\frac{P_S}{N_R}$.

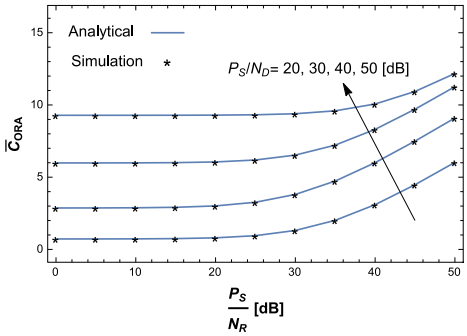

Fig. 6. ACC under ORA vs $\frac{P_S}{N_R}$ for various $\frac{P_S}{N_D}$ values.

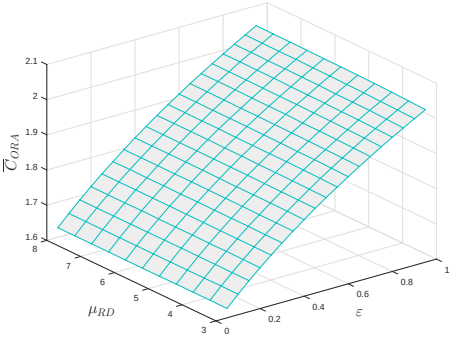

Fig. 7. ACC under ORA vs ε and μ_{RD} for TS.

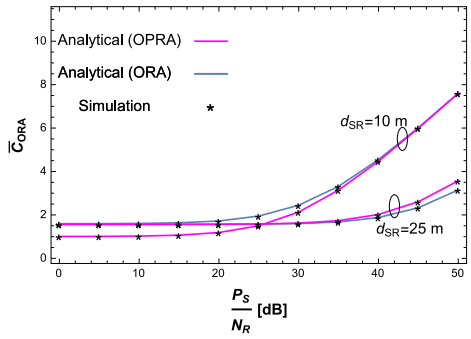

Fig. 8. ACC under ORA and OPRA vs $\frac{P_S}{N_R}$.

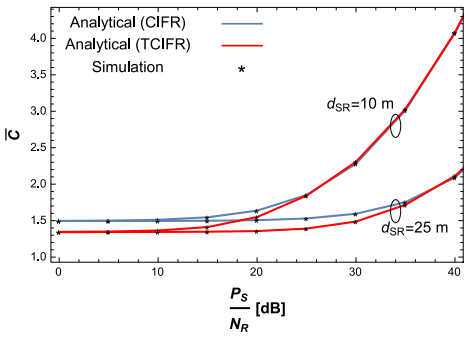

Fig. 9. ACC under CIFR and TCIFR vs $\frac{P_S}{N_R}$ with $\frac{P_S}{N_D} = 25$ dB.

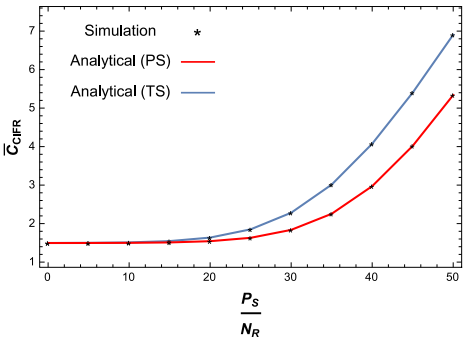

Fig. 10. ACC under CIFR vs $\frac{P_S}{N_R}$ for both TS & PS with $\frac{P_S}{N_D} = 25$ dB.

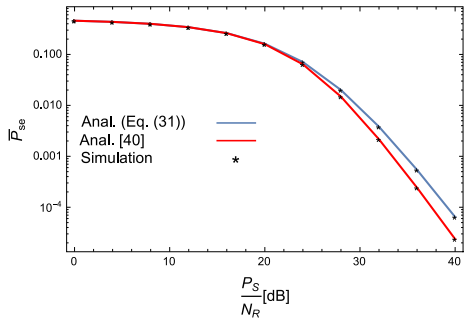

Fig. 11. ASER comparison between the considered system and the one of [40].

Metric	c_s	c_t
ASER (31)	$\frac{1}{\alpha_{RD}}\left(h_{n,p,k}+1\right)$	$-\frac{\mu_{SD}}{2}$
ACC-ORA (36)	$\frac{2}{\alpha_{RD}}\left(h_{n,p,k}+1-\frac{s_p\alpha_{SD}}{4}\right)$	$-\frac{2}{\alpha_{SD}}+s_p, 0<s_p<\frac{2}{\alpha_{SD}}$
ACC-OPRA (41)	$\frac{2}{\alpha_{RD}}\left(h_{n,p,k}+1-\frac{s_p\alpha_{SD}}{4}\right)$	$-\frac{2}{\alpha_{SD}}+s_p, 0<s_p<\frac{2}{\alpha_{SD}}$
ACC-CIFR (46)	$-\frac{3}{\alpha_{SD}}$	
ACC-TCIFR (48)	$\frac{1}{\alpha_{RD}}\left(h_{n,p,k}-1+\frac{\alpha_{SD}\mu_{SD}}{4}\right)$	$-\frac{\mu_{SD}}{2}$

TABLE I: Complex contours definition for the derived metrics' closed-form expressions.

range of SNRs, the combined SNR at the output of the MRC receiver is reduced to the direct link one, and consequently, is irrespective of the first hop parameters and then almost independent of the dual-hop links. This is because the smaller $\frac{P_S}{N_R}$ is, the neglected is the harvested power (less than 2.5 W for the considered parameters' values), leading to a poor dual-hop link.

Fig. 4 shows the ASER performance as a function of $\frac{P_S}{N_R}$, for several values of $\frac{P_S}{N_R}$. Similar to Figs. 2 and 3, it can be noticed that the ASER increases significantly with respect to $\frac{P_S}{N_X}$, $X \in \{R, D\}$. In fact, the greater $\frac{P_S}{N_X}$, the higher γ_{eq} and γ_{SD} are. Thus, γ_T increases as the MRC receiver is used at D. Also, the system's ASER remains below a value of 10^{-5} when $\frac{P_S}{N_X} > 30$ dB, with $X \in \{R, D\}$.

Fig. 5 highlights the ASER evolution versus $\frac{P_S}{N_R}$, as well as the ratio ϱ, for the PS protocol. One can notice evidently that the ASER evolution versus ϱ admits a minimum for a fixed value of $\frac{P_S}{N_R}$, particularly for high $\frac{P_S}{N_R}$ values. This can be explained from (3), where the SNR of the first hop for the PS scheme is affected by the ratio ϱ, whereas for its TS counterpart, the SNR γ_{SR} in (1) is not impacted by the ratio ε.

In Fig. 6, the ACC under ORA policy is shown versus $\frac{P_S}{N_R}$ for various values of $\frac{P_S}{N_D}$, and $d_{SR} = 10$ m. Similarly to the S-R PNR, the ACC increases also significantly by increasing the value $\frac{P_S}{N_D}$. Similarly, Fig. 7 depicts the ACC under ORA policy versus the TS time slot ratio ε as well as the fading parameter μ_{RD}, for $\frac{P_S}{N_D} = 25$ dB. One can ascertain that the ACC increases as a function of ε for the PS protocol, while for the TS case in Fig. 5, the ASER admits a minimum value. This shows that the greater ε is, the higher is the harvested power P_R, and consequently the relay can forward the information signal with a higher power. Interestingly, as TS protocol is employed, even by increasing the duration dedicated to energy harvesting over information decoding one, the received SNR at R is not impacted by ε as can be seen from (1). Nevertheless, for the PS protocol, the first hop's SNR in (3) is affected by the ratio ϱ. In addition to this, the results show that the ACC is not impacted by the fading parameter μ_{RD}.

Fig. 8 shows the ACC performance under ORA and OPRA policies, which are given by (36) and (41), respectively, versus $\frac{P_S}{N_R}$, with $\frac{P_S}{N_D} = 25$ dB. The respective optimal SNR γ^* for the OPRA policy was computed numerically using (44). It can be evidently seen that the overall ACC improves by increasing $\frac{P_S}{N_R}$, corresponding to either a greater radiated power P_S or lower noise power at the relay N_R. Additionally, the result confirms again the free space path-loss effect, due to the propagation distance, on the overall system's performance. Furthermore, it can be evidently seen that ACC under OPRA adaptive policy outperforms slightly its ORA counterpart for $d_{SR} = 25$m, more particularly at high average SNR values. However, it can be noticed that the OPRA policy does not improve the overall system's capacity for a smaller d_{SR} (i.e., 10 m).

Fig. 9 presents the ACC under CIFR and TCIFR policies versus $\frac{P_S}{N_R}$ with $\frac{P_s}{N_D} = 25$ dB, for both TS and PS schemes. One can remark clearly that the ACC under CIFR policy surpasses slightly the TCIFR policy, particularly for average SNR values that are less than 25 dB. Nevertheless, this behavior is changed at high SNR values, where the TCIFR capacity slightly outperforms the CIFR one. In fact, in high average SNR regime, the end-to-end SNR is relatively high. That is, the truncation of the channel inversion does not improve significantly the end-to-end channel capacity. Furthermore, the greater the S-R distance, the higher the free-space path loss, as expected.

The ACC under CIFR policy is plotted for both TS and PS schemes in Fig. 10. Interestingly, one can ascertain from the curves that the TS protocol clearly outperforms its PS counterpart in terms of capacity performance.

Finally, Fig. 11 depicts the ASER of the considered system for BPSK modulation, alongside the one investigated in [40], in which EH is not employed. It is noteworthy that the adopted channel parameters have been chosen to have Rayleigh fading for all links (i.e., $m_{SR} = \mu_{RD} = \mu_{SD} = 1, \alpha_{RD} = \alpha_{SD} = 2$). One can ascertain that the considered SWIPT-based system yields the same ASER performance as that of [40] over a large interval of P_S/N_R values (i.e. $P_S/N_R \leq 20$ dB). This confirms that the same performance is obtained for low and moderate P_S/N_R without the need to have a continuous power source at the relay.

VI. Conclusion

In this paper, a performance analysis of an AF dual-hop energy harvesting-based WCS subject to asymmetric fading channels, namely the Nakagami-m and α-μ, was carried out. Specifically, the MRC receiver was employed at D to combine both direct and dual-hop links, whereas a finite-battery was employed at R. Both SWIPT protocols, namely PS and TS, have been considered in the analysis. Statistical properties such as the CDF and PDF of the end-to-end SNR were retrieved, in generalized expressions for both TS and PS schemes, based on which, closed-form expressions of the ASER as well as ACC over ORA, OPRA, CIFR, and TCIFR adaptive transmission policies, have been derived. These analytical results were corroborated by corresponding Monte Carlo simulations.

The provided results show that the system's ASER is below 10^{-5} when $\frac{P_S}{N_X} > 30$ dB ($X \in \{R, D\}$) for relatively mid-distances. Additionally, the TS protocol clearly outperforms its PS counterpart in terms of capacity performance. Furthermore, the OPRA capacity exhibits better performance compared to its traditional ORA counterpart, particularly at high SNR regime and higher S-R distance. Also, the CIFR scheme generally provides better performance compared to the TCIFR, especially in the low and mid-SNR regimes. Additionally, the system's achievable diversity order depends only on the links' fading severity parameters. Moreover, The Mellin transform of the bivariate FH has been provided for the first time, allowing to retrieve closed-form expressions of most of the considered metrics. From another front, investigating the performance analysis of the considered system by considering variable-gain relaying as well as multi-antenna devices are promising ideas for future works. Furthermore, since the adopted energy harvesting model in this work was a linear one, the investigation of a non-linear energy harvesting scheme is another interesting topic for potential future works.

Appendix A: Proof of Proposition 1

Given the end-to-end SNR expression of the dual-hop link in (9), the respective CDF of γ_{eq} is defined as [32, Eq. (28)]

$$\begin{aligned} F_{\gamma_{eq}}(z) &= \Pr\left[\gamma_{SR} < z\left(1+\frac{C}{\gamma_{RD}}\right)\right] \\ &= \int_0^\infty F_{\gamma_{SR}}\left(z\left(1+\frac{C}{x}\right)\right) f_{\gamma_{RD}}(x)\, dx. \end{aligned} \tag{49}$$

Since γ_{RD} depends on the harvested power P_R, depending on whether $E_R < B_R$ or $E_R \geq B_R$, the CDF of the end-to-end SNR can be expressed as

$$\begin{aligned} F_{\gamma_{eq}}(z) = F_{\gamma_{eq}}(z\,|P_E < P_B)F_{P_E}(P_B) + F_{\gamma_{eq}}(z\,|P_E \geq P_B) \\ \times F^c_{P_E}(P_B). \end{aligned} \tag{50}$$

The conditional PDF of γ_{eq} in each term of the above equation is expressed as

$$F_{\gamma_{eq}}(z\,|P_E < P_B) = \underbrace{\int_0^\infty F_{\gamma_{SR}}\left(z\left(1+\frac{C}{x}\right)\right) f_{\gamma^{(1)}_{RD}}(x)\, dx}_{F_{\gamma^{(1)}_{eq}}(z)}, \tag{51}$$

$$F_{\gamma_{eq}}(z\,|P_E \geq P_B) = \underbrace{\int_0^\infty F_{\gamma_{SR}}\left(z\left(1+\frac{C}{x}\right)\right) f_{\gamma^{(2)}_{RD}}(x)\, dx}_{F_{\gamma^{(2)}_{eq}}(z)}. \tag{52}$$

One can note that evaluating (51) and (52) corresponds to two distinct cases, namely $P_E < P_B$ and $P_E \geq P_B$, respectively.

- *First case:* $P_E < P_B$

One can notice from (6) that $\gamma^{(1)}_{RD}$ is the product of two random variables; namely P_E and Υ_{RD}. Consequently, its PDF is expressed as

$$f_{\gamma^{(1)}_{RD}}(z) = \int_0^\infty \frac{1}{u} f_{P_E}\left(\frac{z}{u}\right) f_{\Upsilon_{RD}}(u)\, du. \tag{53}$$

By involving (12) and (14) into the above equation, as well as using the identity Eq. (07.34.03.0228.01) of [41] alongside with some algebraic manipulations, one obtains

$$\begin{aligned} f_{\gamma^{(1)}_{RD}}(z) = \frac{\alpha_{RD}}{2\Gamma(m_{SR})\Gamma(\mu_{RD})z} \int_0^\infty G^{0,1}_{1,0}\left(\frac{u}{\Psi z}\,\middle|\, \begin{matrix} 1-m_{SR}; - \\ -; - \end{matrix}\right) \\ \times \frac{1}{u} G^{1,0}_{0,1}\left(\mu_{RD}\left(\frac{u}{\overline{\Upsilon}_{RD}}\right)^{\frac{\alpha_{RD}}{2}} \,\middle|\, \begin{matrix} -; - \\ \mu_{RD}; - \end{matrix}\right) du. \end{aligned} \tag{54}$$

where $G^{m,n}_{p,q}(.\,|.)$ is the Meijer's G-function [41, Eq. (07.34.02.0001.01)], and Ψ is defined after (13). Furthermore, using [41, Eqs. (07.34.16.0002.01, 07.34.21.0012.01)] and with some further manipulations, (54) can be expressed as

$$\begin{aligned} f_{\gamma^{(1)}_{RD}}(z) = \frac{\alpha_{RD}}{2\Gamma(m_{SR})\Gamma(\mu_{RD})z} \\ \times H^{2,0}_{0,2}\left(\mu_{RD}\left(\frac{m_{SR}z}{\overline{\gamma}^{(1)}_{RD}}\right)^{\frac{\alpha_{RD}}{2}} \,\middle|\, \begin{matrix} -; - \\ \mathcal{F}; - \end{matrix}\right). \end{aligned} \tag{55}$$

with $\mathcal{F} = \left\{(\mu_{RD}, 1), \left(m_{SR}, \frac{\alpha_{RD}}{2}\right)\right\}$.

Substituting (11) and (55) into (51), and using the finite sum representation of the lower incomplete Gamma function in [34, Eq. (8.352.1)] alongside [37, Eq. (2.9.4)] yields

$$\begin{aligned} F^{(1)}_{\gamma_{eq}}(z) = 1 - \frac{\alpha_{RD} e^{-\frac{m_{SR}}{\overline{\gamma}_{SR}}z}}{2\Gamma(m_{SR})\Gamma(\mu_{RD})} \sum_{n=0}^{m_{SR}-1} \sum_{p=0}^{n} \frac{\left(\frac{m_{SR}}{\overline{\gamma}_{SR}}z\right)^{n-p}}{p!\,(n-p)!} \\ \times \int_0^\infty \frac{1}{x} H^{1,0}_{0,1}\left(\frac{m_{SR}Cz}{\overline{\gamma}_{SR}x}\,\middle|\, \begin{matrix} -; - \\ (p,1); - \end{matrix}\right) \\ \times H^{2,0}_{0,2}\left(\mu_{RD}\left(\frac{m_{SR}x}{\overline{\gamma}^{(1)}_{RD}}\right)^{\frac{\alpha_{RD}}{2}} \,\middle|\, \begin{matrix} -; - \\ \mathcal{F}; - \end{matrix}\right) dx. \end{aligned} \tag{56}$$

Finally, by applying [37, Eqs. (2.1.3, 2.8.4)], one obtains

$$\begin{aligned} F^{(1)}_{\gamma_{eq}}(z) = 1 - \frac{\alpha_{RD}}{2\Gamma(m_{SR})\Gamma(\mu_{RD})} e^{-\frac{m_{SR}}{\overline{\gamma}_{SR}}z} \sum_{n=0}^{m_{SR}-1} \sum_{p=0}^{n} \frac{\left(\frac{m_{SR}}{\overline{\gamma}_{SR}}z\right)^{n-p}}{p!\,(n-p)!} \\ \times H^{3,0}_{0,3}\left(\eta_1\,\middle|\, \begin{matrix} -; - \\ \Delta_1; - \end{matrix}\right), \end{aligned} \tag{57}$$

where η_i $(i = 1, 2)$ and Δ_1 are defined in **Proposition 1.**

- *Second case*: $P_E \geq P_B$

In this scenario, the SNR γ_{RD} is expressed as in (7). Hence, its respective PDF can be derived from (14) using [37, Eq. (2.9.4)] as

$$f_{\gamma^{(2)}_{RD}}(z) = \frac{\alpha_{RD}}{2\Gamma(\mu_{RD})z} H^{1,0}_{0,1}\left(\mu_{RD}\left(\frac{z}{\overline{\gamma}^{(2)}_{RD}}\right)^{\frac{\alpha_{RD}}{2}} \,\middle|\, \begin{matrix} -; - \\ (\mu_{RD}, 1); - \end{matrix}\right). \tag{58}$$

This article has been accepted for publication in a future issue of this journal, but has not been fully edited. Content may change prior to final publication. Citation information: DOI 10.1109/TGCN.2020.3035512, IEEE Transactions on Green Communications and Networking

Similarly to $F^{(1)}_{\gamma_{eq}}(z)$, by involving (11) and the PDF of $\gamma^{(2)}_{RD}$ above into (52), and using [34, Eq. (8.352.1)] jointly with [37, Eq. (2.9.4)], we obtain

$$F_{\gamma^{(2)}_{eq}}(z) = 1 - \frac{\alpha_{RD}}{2\Gamma(\mu_{RD})} e^{-\frac{m_{SR}}{\overline{\gamma}_{SR}}z} \sum_{n=0}^{m_{SR}-1} \sum_{p=0}^{n} \frac{\left(\frac{m_{SR}}{\overline{\gamma}_{SR}}z\right)^{n-p}}{p!(n-p)!} \times \int_0^{\infty} \frac{1}{x} H^{0,1}_{1,0}\left(\frac{\overline{\gamma}_{SR}x}{m_{SR}Cz}\middle| \begin{matrix}(1-p,1);-\\ -;-\end{matrix}\right) \times H^{1,0}_{0,1}\left(\mu_{RD}\left(\frac{x}{\overline{\gamma}^{(2)}_{RD}}\right)^{\frac{\alpha_{RD}}{2}}\middle| \begin{matrix}-;-\\ (\mu_{RD},1);-\end{matrix}\right) dx. \quad (59)$$

By applying [37, Eqs. (2.1.3, 2.8.4)], one obtains

$$F^{(2)}_{\gamma_{eq}}(z) = 1 - \frac{\alpha_{RD} e^{-\frac{m_{SR}}{\overline{\gamma}_{SR}}z}}{2\Gamma(\mu_{RD})} \sum_{n=0}^{m_{SR}-1} \sum_{p=0}^{n} \frac{\left(\frac{m_{SR}}{\overline{\gamma}_{SR}}z\right)^{n-p}}{p!(n-p)!} \times H^{2,0}_{0,2}\left(\eta_2\middle| \begin{matrix}-;-\\ \Delta_2;-\end{matrix}\right), \quad (60)$$

where Δ_2 is defined in **Proposition 1**. Consequently, the CDF of the dual-hop link SNR (i.e., S-R-D) in (50) can be expressed as

$$F_{\gamma_{eq}}(z) = F_{P_E}(P_B) F^{(1)}_{\gamma_{eq}}(z) + F^{c}_{P_E}(P_B) F^{(2)}_{\gamma_{eq}}(z). \quad (61)$$

Given the total SNR γ_T expression in (8), its respective CDF can be expressed as

$$F_{\gamma_T}(z) = \int_0^z F_{\gamma_{eq}}(x) f_{\gamma_{SD}}(z-x)dx. \quad (62)$$

By plugging (15) and (61) into (62), it yields

$$F_{\gamma_T}(z) = F_{P_E}(P_B) F^{(1)}_{\gamma_T}(z) + F^{c}_{P_E}(P_B) F^{(2)}_{\gamma_T}(z), \quad (63)$$

with

$$F^{(i)}_{\gamma_T}(z) = \int_0^z F^{(i)}_{\gamma_{eq}}(x) f_{\gamma_{SD}}(z-x)dx, \quad (64)$$

and

$$F^{(i)}_{\gamma_T}(z) \overset{(a)}{=} \frac{\alpha_{SD}\mu_{SD}^{\mu_{SD}}}{2\Gamma(\mu_{SD})\overline{\gamma}_{SD}} \int_0^z \left[1 - \frac{\alpha_{RD} e^{-\frac{m_{SR}}{\overline{\gamma}_{SR}}x}}{2\left[\Gamma(m_{SR})\right]^{2-i}\Gamma(\mu_{RD})} \times \sum_{n=0}^{m_{SR}-1} \sum_{p=0}^{n} \frac{\left(\frac{m_{SR}}{\overline{\gamma}_{SR}}x\right)^{n-p}}{p!(n-p)!} H^{4-i,0}_{0,4-i}\left(\eta_i x^{\frac{\alpha_{RD}}{2}}\middle| \begin{matrix}-;-\\ \Delta_i;-\end{matrix}\right)\right] \times e^{-\mu_{SD}\left(\frac{z-x}{\overline{\gamma}_D}\right)^{\frac{\alpha_{SD}}{2}}} \left(\frac{z-x}{\overline{\gamma}_{SD}}\right)^{\frac{\alpha_{SD}\mu_{SD}}{2}-1} dx, i = 1,2 \quad (65)$$

$$\overset{(b)}{=} F_{\gamma_{SD}}(z) - \frac{\alpha_{RD}\alpha_{SD}}{4\Gamma(\mu_{RD})\left[\Gamma(m_{SR})\right]^{2-i}\Gamma(\mu_{SD})(2\pi j)^2} \times \sum_{n=0}^{m_{SR}-1} \sum_{p=0}^{n} \sum_{k=0}^{\infty} \frac{(-1)^k \left(\frac{m_{SR}}{\overline{\gamma}_{SR}}\right)^{h_{n,p,k}}}{p!(n-p)!k!} \int_{C_s}\int_{C_t} \Gamma(\mu_{RD}+s) \times \frac{\Gamma\left(p+\frac{\alpha_{RD}}{2}s\right)}{\left[\Gamma\left(m_{SR}+\frac{\alpha_{RD}}{2}s\right)\right]^{i-2}} \Gamma(\mu_{SD}+t) \eta_i^{-s}\vartheta^{-t} \times \int_0^z \frac{x^{n-p+k-\frac{\alpha_{RD}}{2}s}}{(z-x)^{1+\frac{\alpha_{SD}}{2}t}} dxdsdt \quad (66)$$

$$\overset{(c)}{=} F_{\gamma_{SD}}(z) - \frac{\alpha_{RD}\alpha_{SD}}{4\Gamma(\mu_{RD})\left[\Gamma(m_{SR})\right]^{2-i}\Gamma(\mu_{SD})(2\pi j)^2} \times \sum_{n=0}^{m_{SR}-1} \sum_{p=0}^{n} \sum_{k=0}^{\infty} \frac{(-1)^k \left(\frac{m_{SR}}{\overline{\gamma}_{SR}}\right)^{h_{n,p,k}}}{p!(n-p)!k!} \int_{C_s}\int_{C_t} \Gamma(\mu_{RD}+s) \times \frac{\Gamma\left(p+\frac{\alpha_{RD}}{2}s\right)}{\left[\Gamma\left(m_{SR}+\frac{\alpha_{RD}}{2}s\right)\right]^{i-2}} \Gamma(\mu_{SD}+t) \frac{\eta_i^{-s}\vartheta^{-t}}{z^{\frac{\alpha_{RD}}{2}s+\frac{\alpha_{SD}}{2}t-h_{n,p,k}}} \times \mathcal{B}\left(-\frac{\alpha_{SD}}{2}t, h_{n,p,k} - \frac{\alpha_{RD}}{2}s + 1\right) dsdt, \quad (67)$$

where Step (a) holds by involving (15), (57), and (60) into (64), while Step (b) is attained by using the infinite sum representation of $\exp(.)$ in [34, Eq. (1.211.1)] alongside [37, Eq. (2.9.4)] and [37, Eqs. (1.1.1), (1.1.2)], whereas Step (c) holds by using [34, Eq. (3.191.1)]. Finally, by using [34, Eq. (8.384.1)] as well as the bivariate FH definition [35, Eq. (10.1)] and plugging the result into (63), (18) is attained. This concludes the **Proposition**'s proof.

Appendix B: Proof of Corollary 1

By using the residues theorem [37, Theorem (1.2)], the PDF expression in (55) can be expanded at high $\overline{\gamma}^{(i)}_{RD}$ values by the least power of $\mu_{RD}\left(\frac{m_{SR}z}{\overline{\gamma}^{(1)}_{RD}}\right)^{\frac{\alpha_{RD}}{2}}$ as follows

$$f^{(\infty)}_{\gamma^{(1)}_{RD}}(z) \sim \frac{\alpha_{RD}\left(\mu_{RD}\left(\frac{m_{SR}z}{\overline{\gamma}^{(1)}_{RD}}\right)^{\frac{\alpha_{RD}}{2}}\right)^{\min\left(\frac{2m_{SR}}{\alpha_{RD}},\mu_{RD}\right)}}{2\Gamma(m_{SR})\Gamma(\mu_{RD})z}. \quad (68)$$

Additionally, using [41, Eq. (06.06.06.0001.02)] into (11), and involving it alongside (68) into (51), it yields

$$F^{(1,\infty)}_{\gamma_{eq}}(z) = \frac{\alpha_{RD}\left(\frac{m_{SR}}{\overline{\gamma}_{SR}}\right)^{m_{SR}}}{2\Gamma(m_{SR})\Gamma(\mu_{RD})\Gamma(m_{SR}+1)} \int_0^{\infty} \frac{\left(z\left(1+\frac{C}{x}\right)\right)^{m_{SR}}}{x} \times \left(\mu_{RD}\left(\frac{m_{SR}x}{\overline{\gamma}^{(1)}_{RD}}\right)^{\frac{\alpha_{RD}}{2}}\right)^{\min\left(\frac{2m_{SR}}{\alpha_{RD}},\mu_{RD}\right)} dx. \quad (69)$$

Therefore, by using the change of variables $u = 1 + \frac{C}{x}$, one obtains

$$F^{(1,\infty)}_{\gamma_{eq}}(z) \sim \frac{C^{\min\left(m_{SR},\frac{\alpha_{RD}\mu_{RD}}{2}\right)}\alpha_{RD}\left(\frac{m_{SR}}{\overline{\gamma}_{SR}}\right)^{m_{SR}}}{2\Gamma(m_{SR})\Gamma(\mu_{RD})\Gamma(m_{SR}+1)} \times \left(\mu_{RD}\left(\frac{m_{SR}}{\overline{\gamma}^{(1)}_{RD}}\right)^{\frac{\alpha_{RD}}{2}}\right)^{\min\left(\frac{2m_{SR}}{\alpha_{RD}},\mu_{RD}\right)} z^{m_{SR}} \times \int_{u=1}^{\infty} \frac{u^{m_{SR}}}{(u-1)^{1+\min\left(m_{SR},\frac{\alpha_{RD}\mu_{RD}}{2}\right)}} du. \quad (70)$$

From another front, at high $\overline{\gamma}_{SD}$ values, the PDF in (15) is expanded as

$$f^{(\infty)}_{\gamma_{SD}}(z) \sim \frac{\alpha_{SD}\mu_{SD}^{\mu_{SD}}}{2\Gamma(\mu_{SD})\overline{\gamma}_{SD}^{\frac{\alpha_{SD}\mu_{SD}}{2}}} z^{\frac{\alpha_{SD}\mu_{SD}}{2}-1}. \quad (71)$$

This article has been accepted for publication in a future issue of this journal, but has not been fully edited. Content may change prior to final publication. Citation information: DOI 10.1109/TGCN.2020.3035512, IEEE Transactions on Green Communications and Networking

Therefore, by involving (71) and (70) into (64), one gets

$$F_{\gamma_T}^{(1,\infty)}(z) \sim \frac{\alpha_{RD}\alpha_{SD}\mu_{SD}^{\mu_{SD}} C^{\min\left(m_{SR},\frac{\alpha_{RD}\mu_{RD}}{2}\right)}}{4\Gamma(\mu_{SD})\Gamma(m_{SR})\Gamma(\mu_{RD})\Gamma(m_{SR}+1)} \times \left(\mu_{RD}\left(\frac{m_{SR}}{\overline{\gamma}_{RD}^{(1)}}\right)^{\frac{\alpha_{RD}}{2}}\right)^{\min\left(\frac{2m_{SR}}{\alpha_{RD}},\mu_{RD}\right)} \times \frac{\left(\frac{m_{SR}}{\overline{\gamma}_{SR}}\right)^{m_{SR}}}{\overline{\gamma}_{SD}^{\frac{\alpha_{SD}\mu_{SD}}{2}}} \int_{x=0}^{z} \frac{x^{m_{SR}}}{(z-x)^{1-\frac{\alpha_{SD}\mu_{SD}}{2}}} \times \int_{u=1}^{\infty} \frac{u^{m_{SR}}}{(u-1)^{1+\min\left(m_{SR},\frac{\alpha_{RD}\mu_{RD}}{2}\right)}} dxdu. \quad (72)$$

Moreover, given that the double integral in (72) and its counterpart $F_{\gamma_T}^{(2,\infty)}(z)$ are independent of the average SNRs, it follows that the system's achievable diversity order is irrespective of these two double integrals. Thus, when $\overline{\gamma}_{SR} = \overline{\gamma}_{RD}^{(i)} = \overline{\gamma}_{SD} = \overline{\gamma}$, (20) is attained.

Appendix C: Proof of Lemma 1

The moment of order $n = -1$ of γ_T is defined in terms of its CDF as follows

$$\mathbb{E}_{\gamma_T}\left[\gamma_T^{-1}\right] = \int_0^{\infty} \frac{F_{\gamma_T}(z)}{z^2} dz. \quad (73)$$

By involving (18) into the integral in (73), it yields (21) with

$$\mathcal{K}_{SD} = \int_0^{\infty} \frac{F_{\gamma_{SD}}(z)}{z^2} dz, \quad (74)$$

and

$$\mathcal{Y}_i = \int_0^{\infty} \frac{T_i(z)}{z^2} dz. \quad (75)$$

Therefore, we have the following

$$\mathcal{K}_{SD} \overset{(a)}{=} \frac{1}{\Gamma(\mu_{SD})} \int_0^{\infty} z^{-2}\gamma_{inc}\left(\mu_{SD}, \vartheta z^{\frac{\alpha_{SD}}{2}}\right) dz, \quad (76)$$

$$\overset{(b)}{=} \frac{2}{\alpha_{SD}\Gamma(\mu_{SD})} \int_0^{\infty} x^{-\frac{2}{\alpha_{SD}}-1} \times G_{1,2}^{1,1}\left(\vartheta x \middle| \begin{matrix} 1; - \\ \mu_{SD}; 0 \end{matrix}\right) dx, \quad (77)$$

where Step (a) is obtained by involving the CDF in (17) into (74), while Step (b) is reached via [41, Eq. (06.06.26.0004.01)] alongside the change of variable $x = z^{\frac{\alpha_{SD}}{2}}$. Finally, using the Mellin transform [37, Eq. (2.5.12)], (22) is reached. On the other hand, we have also

$$\mathcal{Y}_i \overset{(a)}{=} \frac{\alpha_{RD}\alpha_{SD}}{4\Gamma(\mu_{SD})\Gamma(m_{SR})\Gamma(\mu_{RD})} \frac{1}{2\pi j} \sum_{n=0}^{m_{SR}-1} \sum_{p=0}^{n} \frac{1}{p!(n-p)!} \times \sum_{k=0}^{\infty} \frac{(-1)^k}{k!} \left(\frac{m_{SR}}{\overline{\gamma}_{SR}}\right)^{h_{n,p,k}} \int_{C_t} \Gamma(\mu_{SD}+t) \times \Gamma\left(-\frac{\alpha_{SD}}{2}t\right) \vartheta^{-t} \int_0^{\infty} z^{h_{n,p,k}-\frac{\alpha_{SD}}{2}t-2} \times H_{1,4}^{3,1}\left(\eta_i z^{\frac{\alpha_{RD}}{2}} \middle| \begin{matrix} \mathcal{E}_2; - \\ \Delta_i; \left(-h_{n,p,k}+\frac{\alpha_{SD}}{2}t, \frac{\alpha_{RD}}{2}\right) \end{matrix}\right) dzdsdt, \quad (78)$$

$$\overset{(b)}{=} \frac{\eta_i^{\frac{2}{\alpha_{RD}}}\alpha_{SD}}{2\Gamma(\mu_{SD})\Gamma(\mu_{RD})} \frac{1}{2\pi j} \sum_{n=0}^{m_{SR}-1} \sum_{p=0}^{n} \sum_{k=0}^{\infty} \frac{(-1)^k}{p!(n-p)!k!} \times \left(\frac{\overline{\gamma}_{RD}^{(i)}}{m_{SR}^{2-i} C \mu_{RD}^{\frac{2}{\alpha_{RD}}}}\right)^{h_{n,p,k}} \int_{C_t} \Gamma\left(m_{SR}+h_{n,p,k}-\frac{\alpha_{SD}}{2}t-1\right) \times \Gamma(\mu_{SD}+t)\Gamma\left(\mu_{RD}+\frac{2}{\alpha_{RD}}\left(h_{n,p,k}-\frac{\alpha_{SD}}{2}t-1\right)\right) \times \frac{\Gamma\left(-\frac{\alpha_{SD}}{2}t\right)\Gamma\left(n+k-\frac{\alpha_{SD}}{2}t-1\right)}{\Gamma\left(2+\frac{\alpha_{SD}}{2}t\right)} \left(\frac{\vartheta^{\frac{2}{\alpha_{SD}}}}{\eta_i^{\frac{2}{\alpha_{RD}}}}\right)^{-\frac{\alpha_{SD}}{2}t} dsdt, \quad (79)$$

where Step (a) is reached by substituting (19) into (75), and using [37, Eqs. (1.1.1, 1.1.2)] and [35, Eq. (10.1)], while the Mellin transform of the bivariate FH is computed in Step (b) using [37, Eq. (2.5.12)]. Finally, using [37, Eqs. (1.1.1, 1.1.2)], we get (23). This concludes the proof of **Lemma 1**.

Appendix D: Proof of Corollary 2

The integral $\mathcal{I}(x) = \int_x^{\infty} \frac{f_{\gamma_T}(z)}{z} dz$ can be written, using integration by parts, as follows

$$\mathcal{I}(x) = \int_0^{\infty} \frac{F_{\gamma_T}(z)}{z^2} dz - \int_0^{x} \frac{F_{\gamma_T}(z)}{z^2} dz - \frac{F_{\gamma_T}(x)}{x}, \quad (80)$$

where $\int_0^{\infty} \frac{F_{\gamma_T}(z)}{z^2} dz = \mathbb{E}\left[\gamma_T^{-1}\right]$ is given in (21). Next, by plugging (18) into the second term of (80), it yields

$$\int_0^{x} \frac{F_{\gamma_T}(z)}{z^2} dz = \mathcal{M}_{SD}(x) - \frac{F_{P_E}(P_B)}{\Gamma(m_{SR})}\mathcal{W}_1(x) - F_{P_E}^{c}(P_B)\mathcal{W}_2(x), \quad (81)$$

with

$$\mathcal{M}_{SD}(x) \overset{(a)}{=} \frac{1}{\Gamma(\mu_{SD})} \int_0^{x} \frac{\gamma_{inc}\left(\mu_{SD}, \vartheta z^{\frac{\alpha_{SD}}{2}}\right)}{z^2} dz, \quad (82)$$

$$\overset{(b)}{=} \frac{2}{\alpha_{SD}\Gamma(\mu_{SD})} \int_0^{x^{\frac{\alpha_{SD}}{2}}} \frac{G_{1,2}^{1,1}\left(\vartheta^{\frac{2}{\alpha_{SD}}}u \middle| \begin{matrix} 1; - \\ \mu_{SD}; 0 \end{matrix}\right)}{u^{\frac{2}{\alpha_{SD}}+1}} du, \quad (83)$$

where Step (a) is reached by involving (17) into the second term of (80), while Step (b) is obtained through the change of variable $u = z^{\frac{\alpha_{SD}}{2}}$ alongside [41, Eq. (06.06.26.0004.01)]. Finally, using [41, Eq. (07.34.21.0003.01)], (27) is reached.

This article has been accepted for publication in a future issue of this journal, but has not been fully edited. Content may change prior to final publication. Citation information: DOI 10.1109/TGCN.2020.3035512, IEEE Transactions on Green Communications and Networking

On the other hand, we have

$$\mathcal{W}_i(x) \overset{(a)}{=} \int_0^x \frac{T_i(z)}{z^2} \tag{84}$$

$$\overset{(b)}{=} \frac{\alpha_{RD}\alpha_{SD}}{4\Gamma(\mu_{SD})\Gamma(\mu_{RD})\left(2\pi j\right)^2 x} \sum_{n=0}^{m_{SR}-1}\sum_{p=0}^{n}\sum_{k=0}^{\infty}\frac{(-1)^k}{p!(n-p)!k!} \times \left(\frac{m_{SR}x}{\overline{\gamma}_{SR}}\right)^{h_{\,n,p,k}} \int_{C_s}\int_{C_t} \frac{\Gamma\left(h_{\,n,p,k}-\frac{\alpha_{RD}}{2}s-\frac{\alpha_{SD}}{2}t-2\right)}{\Gamma\left(1+h_{\,n,p,k}-\frac{\alpha_{SD}}{2}t-\frac{\alpha_{RD}}{2}s\right)} \times \frac{\Gamma\left(\mu_{RD}+s\right)\Gamma\left(1+h_{\,n,p,k}-\frac{\alpha_{RD}}{2}s\right)\Gamma\left(p+\frac{\alpha_{RD}}{2}s\right)}{\Gamma\left(h_{\,n,p,k}-\frac{\alpha_{RD}}{2}s-\frac{\alpha_{SD}}{2}t-1\right)\left[\Gamma\left(m_{SR}+\frac{\alpha_{RD}}{2}s\right)\right]^{i-2}} \times \Gamma\left(-\frac{\alpha_{SD}}{2}t\right)\Gamma\left(\mu_{SD}+t\right)\left(\eta_i x^{\frac{\alpha_{RD}}{2}}\right)^{-s}\left(\vartheta x^{\frac{\alpha_{SD}}{2}}\right)^{-t} dsdt, \tag{85}$$

where Step (a) is obtained by plugging (19) into the second term of (80), while Step (b) holds by using the bivariate FH definition [35, Eqs. (10.1-10.4)] on (84) alongside [34, Eq. (8.331.1)]. Finally, using [37, Eqs. (1.1.1, 1.1.2)], we get (28).

Appendix E: Proof of Proposition 2

By using the integration by parts in (30) alongside [34, Eqs. (8.250.1, 8.250.4)], the ASER can be rewritten as

$$\overline{P}_{se} = \rho\sqrt{\frac{\tau}{\pi}}\int_0^\infty z^{\frac{-1}{2}}e^{-\tau z}F_{\gamma_T}(z)dz. \tag{86}$$

By involving the CDF in (18) into (86), one obtains

$$\overline{P}_{se}(z) = \frac{\rho}{\sqrt{\pi}}\left(\mathcal{H}_{SD}-\mathcal{V}_1-\mathcal{V}_2\right), \tag{87}$$

with

$$\mathcal{H}_{SD} = \sqrt{\tau}\int_0^\infty z^{\frac{-1}{2}}e^{-\tau z}F_{\gamma_{SD}}(z)dz, \tag{88}$$

$$\mathcal{V}_i = \frac{F_{P_E}\left(P_B\right)\sqrt{\tau}}{\Gamma(m_{SR})}\int_0^\infty z^{\frac{-1}{2}}e^{-\tau z}T_i(z); i=1,2. \tag{89}$$

By involving (17) into (88) as well using [41, Eq. (06.06.26.0004.01)] alongside [42, Eq. (2.19)], (32) is attained. On the other hand, by plugging (19) into (89), it produces

$$\mathcal{V}_i \overset{(a)}{=} \frac{\sqrt{\tau}\alpha_{RD}\alpha_{SD}}{4\Gamma(\mu_{SD})\Gamma(\mu_{RD})\left(2\pi j\right)^2}\sum_{n=0}^{m_{SR}-1}\sum_{p=0}^{n}\sum_{k=0}^{\infty}\frac{(-1)^k}{p!(n-p)!k!} \times \left(\frac{m_{SR}}{\overline{\gamma}_{SR}}\right)^{h_{\,n,p,k}}\int_{C_s}\int_{C_t}\frac{\Gamma\left(\mu_{RD}+s\right)\Gamma\left(p+\frac{\alpha_{RD}}{2}s\right)}{\left[\Gamma\left(m_{SR}+\frac{\alpha_{RD}}{2}s\right)\right]^{i-2}} \times \frac{\Gamma\left(1+h_{\,n,p,k}-\frac{\alpha_{RD}}{2}s\right)\Gamma\left(\mu_{SD}+t\right)\Gamma\left(-\frac{\alpha_{SD}}{2}t\right)}{\Gamma\left(1+h_{\,n,p,k}-\frac{\alpha_{RD}}{2}s-\frac{\alpha_{SD}}{2}t\right)} \times \eta_i^{-s}\vartheta^{-t}\int_0^\infty e^{-\tau z}z^{h_{\,n,p,k}-\frac{1}{2}-\frac{\alpha_{RD}}{2}s-\frac{\alpha_{SD}}{2}t}dsdtdz, \tag{90}$$

$$\overset{(b)}{=} \frac{\alpha_{RD}\alpha_{SD}}{4\Gamma(\mu_{SD})\Gamma(\mu_{RD})\left(2\pi j\right)^2}\sum_{n=0}^{m_{SR}-1}\sum_{p=0}^{n}\sum_{k=0}^{\infty}\frac{(-1)^k}{p!(n-p)!k!} \times \left(\frac{m_{SR}}{\overline{\gamma}_{SR}\tau}\right)^{h_{\,n,p,k}}\int_{C_s}\int_{C_t}\frac{\Gamma\left(h_{\,n,p,k}+\frac{1}{2}-\frac{\alpha_{RD}}{2}s-\frac{\alpha_{SD}}{2}t\right)}{\Gamma\left(h_{\,n,p,k}+1-\frac{\alpha_{RD}}{2}s-\frac{\alpha_{SD}}{2}t\right)} \times \frac{\Gamma\left(\mu_{RD}+s\right)\Gamma\left(p+\frac{\alpha_{RD}}{2}s\right)\Gamma\left(h_{\,n,p,k}+1-\frac{\alpha_{RD}}{2}s\right)}{\left[\Gamma\left(m_{SR}+\frac{\alpha_{RD}}{2}s\right)\right]^{i-2}} \times \Gamma\left(\mu_{SD}+t\right)\Gamma\left(-\frac{\alpha_{SD}}{2}t\right)\left(\frac{\eta_i}{\tau^{\frac{\alpha_{RD}}{2}}}\right)^{-s}\left(\frac{\vartheta}{\tau^{\frac{\alpha_{SD}}{2}}}\right)^{-t}dsdt, \tag{91}$$

where Step (a) is obtained by using the bivariate FH definition of T_i [35, Eq. (10.1)], and Step (b) is reached through the use of [34, Eq. (3.381.4)] and through performing some algebraic manipulations. Finally, using once more [35, Eq. (10.1)], (33) is reached. This concludes the proof of **Corollary 2**.

Appendix F: Proof of Proposition 3

By plugging (18) into (35), it yields (36) where

$$\mathcal{G}_{SD} = \frac{1}{\Gamma(\mu_{SD})}\int_0^\infty \frac{\Gamma\left(\mu_{SD},\vartheta z^{\frac{\alpha_{SD}}{2}}\right)}{1+z}dz, \tag{92}$$

and

$$\mathcal{X}_i = \int_0^\infty \frac{T_i(z)}{1+z}dz$$

Thus, by involving [41, Eqs. (07.34.03.0271.01, 06.06.26.0005.01)] into (92) alongside [37, Eq. (2.8.4)], (37) is attained. Furthermore, we have the following

$$\mathcal{X}_i \overset{(a)}{=} \frac{\alpha_{RD}\alpha_{SD}}{4\Gamma(\mu_{SD})\Gamma(m_{SR})\Gamma(\mu_{RD})\left(2\pi j\right)^2}\sum_{n=0}^{m_{SR}-1}\sum_{p=0}^{n}\frac{1}{p!(n-p)!} \times \sum_{k=0}^{\infty}\frac{(-1)^k}{k!}\left(\frac{m_{SR}}{\overline{\gamma}_{SR}}\right)^{h_{n,p,k}}\int_{C_s}\int_{C_t}\Gamma\left(h_{\,n,p,k}+1-\frac{\alpha_{RD}}{2}s\right) \times \frac{\Gamma\left(\mu_{RD}+s\right)\Gamma\left(p+\frac{\alpha_{RD}}{2}s\right)\Gamma\left(\mu_{SD}+t\right)\Gamma\left(-\frac{\alpha_{SD}}{2}t\right)}{\left[\Gamma\left(m_{SR}+\frac{\alpha_{RD}}{2}s\right)\right]^{i-2}\Gamma\left(h_{\,n,p,k}+1-\frac{\alpha_{RD}}{2}s-\frac{\alpha_{SD}}{2}t\right)} \times \eta_i^{-s}\vartheta^{-t}\int_0^\infty \frac{G_{1,1}^{1,1}\left(z\,\middle|\,\begin{matrix}0;-\\0;-\end{matrix}\right)}{z^{\frac{\alpha_{RD}}{2}s+\frac{\alpha_{SD}}{2}t-h_{\,n,p,k}}}dsdtdz, \tag{93}$$

$$\overset{(b)}{=} \frac{\alpha_{RD}\alpha_{SD}}{4\Gamma(\mu_{SD})\Gamma(m_{SR})\Gamma(\mu_{RD})\left(2\pi j\right)^2}\sum_{n=0}^{m_{SR}-1}\sum_{p=0}^{n}\frac{1}{p!(n-p)!} \times \sum_{k=0}^{\infty}\frac{(-1)^k}{k!}\left(\frac{m_{SR}}{\overline{\gamma}_{SR}}\right)^{h_{n,p,k}}\int_{C_s}\int_{C_t}\frac{\Gamma\left(1+h_{n,p,k}-\frac{\alpha_{RD}}{2}s\right)}{\left[\Gamma\left(m_{SR}+\frac{\alpha_{RD}}{2}s\right)\right]^{i-2}} \times \Gamma\left(\mu_{RD}+s\right)\Gamma\left(p+\frac{\alpha_{RD}}{2}s\right)\Gamma\left(-\frac{\alpha_{SD}}{2}t\right)\Gamma\left(\mu_{SD}+t\right) \times \Gamma\left(-h_{n,p,k}+\frac{\alpha_{RD}}{2}s+\frac{\alpha_{SD}}{2}t\right)\eta_i^{-s}\vartheta^{-t}dsdt. \tag{94}$$

Here, Step (a) is attained by using the bivariate FH definition of $T_i(z)$ [35, Eq. (10.1)] along with [41, Eq. (07.34.03.0271.01)], while Step (b) is reached through the aid of the Mellin transform [42, Eq. (2.9)]. Finally, using [35, Eq. (10.1)], (38) is reached.

This article has been accepted for publication in a future issue of this journal, but has not been fully edited. Content may change prior to final publication. Citation information: DOI 10.1109/TGCN.2020.3035512, IEEE Transactions on Green Communications and Networking

APPENDIX G: PROOF OF PROPOSITION 4

The ACC under OPRA policy can be alternatively written as

$$\overline{C}_{OPRA} = \frac{1}{\log(2)} \int_{\gamma^*}^{\infty} \frac{1}{z} F^c_{\gamma_T}(z) dz. \tag{95}$$

By plugging (18) into (95), one obtains

$$\mathcal{O}_{SD}\left(\gamma^*\right) = \int_{\gamma^*}^{\infty} \frac{F^c_{\gamma_{SD}}(z)}{z} dz, \tag{96}$$

and

$$\mathcal{N}_i\left(\gamma^*\right) = \int_{\gamma^*}^{\infty} \frac{T_i(z)}{z} dz, \tag{97}$$

with $\mathcal{E}_1$ and $\mathcal{E}_2$ are given in **Proposition 1**. It follows that

$$\mathcal{O}_{SD}\left(\gamma^*\right) \overset{(a)}{=} \frac{1}{\gamma^* \Gamma(\mu_{SD})} \int_0^{\infty} \frac{\Gamma\left(\mu_{SD}, \vartheta\left(\gamma^*\left(u+1\right)\right)^{\frac{\alpha_{SD}}{2}}\right)}{u+1} du \tag{98}$$

$$\overset{(b)}{=} \frac{1}{\Gamma(\mu_{SD})} \frac{1}{2\pi j} \int_{C_s} \frac{\Gamma\left(\mu_{SD}+s\right)\Gamma\left(s\right)}{\Gamma\left(1+s\right)} \left(\vartheta\left(\gamma^*\right)^{\frac{\alpha_{SD}}{2}}\right)^{-s} \times \int_0^{\infty} \frac{1}{\left(u+1\right)^{\frac{\alpha_{SD}}{2}s+1}} du ds \tag{99}$$

$$\overset{(c)}{=} \frac{1}{2\pi j \Gamma(\mu_{SD})} \int_{C_s} \frac{\Gamma\left(\frac{\alpha_{SD}}{2}s\right)\Gamma\left(\mu_{SD}+s\right)\Gamma\left(s\right)}{\Gamma\left(\frac{\alpha_{SD}}{2}s+1\right)\Gamma\left(1+s\right)} \times \left(\vartheta\left(\gamma^*\right)^{\frac{\alpha_{SD}}{2}}\right)^{-s} ds, \tag{100}$$

where Step (a) holds by incorporating (17) into (96) alongside the change of variable $u = \frac{z}{\gamma^*} - 1$. Next, Step (b) is produced using [41, Eq. (06.06.26.0005.01)] jointly with [42, Eq. (1.112)], whereas Step (c) is attained by using [34, Eq. (3.194.3)]. Finally, using [42, Eq. (1.112)], (42) is obtained.

On the other hand, we have

$$\mathcal{N}_i\left(\gamma^*\right) \overset{(a)}{=} \frac{\alpha_{RD}\alpha_{SD}}{4\Gamma(\mu_{SD})\Gamma(\mu_{RD})\left(2\pi j\right)^2} \sum_{n=0}^{m_{SR}-1} \sum_{p=0}^{n} \frac{1}{p!(n-p)!} \times \sum_{k=0}^{\infty} \frac{(-1)^k}{k!} \left(\frac{m_{SR}\gamma^*}{\overline{\gamma}_{SR}}\right)^{h_{n,p,k}} \int_{C_s}\int_{C_t} \Gamma\left(p+\frac{\alpha_{RD}}{2}s\right) \times \frac{\Gamma\left(\mu_{RD}+s\right)\Gamma\left(h_{\,n,p,k}+1-\frac{\alpha_{RD}}{2}s\right)}{\left[\Gamma\left(m_{SR}+\frac{\alpha_{RD}}{2}s\right)\right]^{i-2}\Gamma\left(1+h_{n,p,k}-\frac{\alpha_{RD}}{2}s-\frac{\alpha_{SD}}{2}t\right)} \times \Gamma\left(-\frac{\alpha_{SD}}{2}t\right)\Gamma\left(\mu_{SD}+t\right)\left(\eta_i\left(\gamma^*\right)^{\frac{\alpha_{RD}}{2}}\right)^{-s}\left(\vartheta\left(\gamma^*\right)^{\frac{\alpha_{SD}}{2}}\right)^{-t} \times \int_0^{\infty} \left(1+u\right)^{h_{\,n,p,k}-1-\frac{\alpha_{RD}}{2}s-\frac{\alpha_{SD}}{2}t} du ds dt, \tag{101}$$

$$\overset{(b)}{=} \frac{\alpha_{RD}\alpha_{SD}}{4\Gamma(\mu_{SD})\Gamma(m_{SR})\Gamma(\mu_{RD})\left(2\pi j\right)^2} \sum_{n=0}^{m_{SR}-1} \sum_{p=0}^{n} \frac{1}{p!(n-p)!} \times \sum_{k=0}^{\infty} \frac{(-1)^k}{k!} \left(\frac{m_{SR}\gamma^*}{\overline{\gamma}_{SR}}\right)^{h_{n,p,k}} \int_{C_s}\int_{C_t} \Gamma\left(p+\frac{\alpha_{RD}}{2}s\right) \times \frac{\Gamma\left(\mu_{RD}+s\right)\Gamma\left(h_{\,n,p,k}+1-\frac{\alpha_{RD}}{2}s\right)}{\left[\Gamma\left(m_{SR}+\frac{\alpha_{RD}}{2}s\right)\right]^{i-2}} \times \Gamma\left(\mu_{SD}+t\right)\Gamma\left(-\frac{\alpha_{SD}}{2}t\right)\frac{\Gamma\left(-h_{\,n,p,k}+\frac{\alpha_{RD}}{2}s+\frac{\alpha_{SD}}{2}t\right)}{\Gamma\left(1+h_{\,n,p,k}-\frac{\alpha_{RD}}{2}s-\frac{\alpha_{SD}}{2}t\right)} \times \frac{\left(\eta_i\left(\gamma^*\right)^{\frac{\alpha_{RD}}{2}}\right)^{-s}}{\Gamma\left(-h_{\,n,p,k}+\frac{\alpha_{RD}}{2}s+\frac{\alpha_{SD}}{2}t+1\right)}\left(\vartheta\left(\gamma^*\right)^{\frac{\alpha_{SD}}{2}}\right)^{-t} ds dt. \tag{102}$$

Again, Step (a) holds by using the bivariate FH definition of $T_i(z)$ [35, Eq. (10.1)] jointly with the change of variable $u = \frac{z}{\gamma^*} - 1$, while Step (b) follows from [34, Eqs. (3.194.3, 8.384.1)]. Lastly, using [35, Eqs. (10.1-10.4)], (43) is attained.

On the other hand, the optimal cutoff SNR γ^* is defined as the zero of the following function

$$g(x) = \frac{F^c_{\gamma_T}(x)}{x} - \int_x^{\infty} \frac{f_{\gamma_T}(z)dz}{z} - 1, \tag{103}$$

By differentiating (103) with respect to x, and computing its limits at 0 and ∞ it yields

$$g'(x) = -\frac{F^c_{\gamma_{eq}}(x)}{x^2} < 0, \tag{104}$$

and

$$\lim_{x\to 0} g\left(x\right) = \infty, \lim_{x\to\infty} g\left(x\right) = -1. \tag{105}$$

Given the above, the zero value of (40) is unique. Moreover, by plugging (24) into (103), (40) is achieved.

REFERENCES

[1] L. Jiang, H. Tian, Z. Xing, K. Wang, K. Zhang, S. Maharjan, S. Gjessing, and Y. Zhang, "Social-aware energy harvesting device-to-device communications in 5G networks," *IEEE Wireless Commun.*, vol. 23, no. 4, pp. 20–27, Aug. 2016.

[2] Y. Zhang, R. Yu, M. Nekovee, Y. Liu, S. Xie, and S. Gjessing, "Cognitive machine-to-machine communications: visions and potentials for the smart grid," *IEEE Netw.*, vol. 26, no. 3, pp. 6–13, May 2012.

[3] Y. Zhang, J. Ge, and E. Serpedin, "Performance analysis of a 5G energy-constrained downlink relaying network with non-orthogonal multiple access," *IEEE Trans. Wireless Commun.*, vol. 16, no. 12, pp. 8333–8346, Dec 2017.

[4] M. A. Abd-Elmagid, T. A. ElBatt, and K. G. Seddik, "Optimization of energy-constrained wireless powered communication networks with heterogeneous nodes," *Wireless Networks J.*, vol. 25, pp. 713–730, Sep. 2017.

[5] E. Hossain and M. Hasan, "5G cellular: key enabling technologies and research challenges," *IEEE Instrum. Meas. Mag.*, vol. 18, no. 3, pp. 11–21, June 2015.

[6] G. Pan, H. Lei, Y. Yuan, and Z. Ding, "Performance analysis and optimization for SWIPT wireless sensor networks," *IEEE Trans. Commun.*, vol. 65, no. 5, pp. 2291–2302, May 2017.

[7] S. Sudevalayam and P. Kulkarni, "Energy harvesting sensor nodes: Survey and implications," *IEEE Commun. Surveys Tuts.*, vol. 13, no. 3, pp. 443–461, Jul. 2011.

[8] P. Kamalinejad, C. Mahapatra, Z. Sheng, S. Mirabbasi, V. C. M. Leung, and Y. L. Guan, "Wireless energy harvesting for the internet of things," *IEEE Commun. Mag.*, vol. 53, no. 6, pp. 102–108, Jun. 2015.

[9] J. Ye, H. Lei, Y. Liu, G. Pan, D. B. da Costa, Q. Ni, and Z. Ding, "Cooperative communications with wireless energy harvesting over Nakagami- m fading channels," *IEEE Trans. Commun.*, vol. 65, no. 12, pp. 5149–5164, Dec. 2017.

[10] D. Niyato, D. I. Kim, M. Maso, and Z. Han, "Wireless powered communication networks: Research directions and technological approaches," *IEEE Wireless Commun.*, vol. 24, no. 6, pp. 88–97, Dec. 2017.

[11] Y. Gu and S. Aïssa, "RF-based energy harvesting in decode-and-forward relaying systems: Ergodic and outage capacities," *IEEE Trans. Wireless Commun.*, vol. 14, no. 11, pp. 6425–6434, Nov. 2015.

[12] M.-K. Simon and M.-S. Alouini, *Digital Communication Over Fading Channels*. New York: John Wiley and Sons, 2005.

[13] M. D. Yacoub, "The α-μ distribution: A physical fading model for the Stacy distribution," *IEEE Trans. Veh. Technol.*, vol. 56, no. 1, pp. 27–34, Jan. 2007.

[14] P. C. Sofotasios, M. K. Fikadu, S. Muhaidat, S. Freear, G. K. Karagiannidis, and M. Valkama, "Relay selection based full-duplex cooperative systems under adaptive transmission," *IEEE Wireless Commun. Lett.*, vol. 6, no. 5, pp. 602–605, Oct. 2017.

[15] M. K. Fikadu, P. C. Sofotasios, Q. Cui, G. K. Karagiannidis, and M. Valkama, "Exact error analysis and energy efficiency optimization of regenerative relay systems under spatial correlation," *IEEE Trans. Veh. Tech.*, vol. 65, no. 7, pp. 4973–4992, Jul. 2016.

[16] M. K. Fikadu, P. C. Sofotasios, S. Muhaidat, Q. Cui, G. K. Karagiannidis, and M. Valkama, "Error rate and power allocation analysis of regenerative networks over generalized fading channels," *IEEE Trans. Commun.*, vol. 64, no. 4, pp. 1751–1768, Apr. 2016.

[17] M. O. Hasna and M. S. Alouini, "A performance study of dual-hop transmissions with fixed gain relays," *IEEE Trans. Wireless Commun.*, vol. 3, no. 6, pp. 1963–1968, Nov. 2004.

[18] P. C. Sofotasios, M. K. Fikadu, S. Muhaidat, Q. Cui, G. K. Karagiannidis, and M. Valkama, "Full-duplex regenerative relaying and energy-efficiency optimization over generalized asymmetric fading channels," *IEEE Trans. Wireless Commun.*, vol. 16, no. 5, pp. 3232–3251, May 2017.

[19] N. Kapucu, M. Bilim, and I. Develi, "Outage probability analysis of dual-hop decode-and-forward relaying over mixed Rayleigh and generalized Gamma fading channels," *Wireless Pers. Commun.*, vol. 71, no. 2, pp. 947–954, Jul. 2013.

[20] H. A. Suraweera, R. H. Y. Louie, Y. Li, G. K. Karagiannidis, and B. Vucetic, "Two hop amplify-and-forward transmission in mixed Rayleigh and Rician fading channels," *IEEE Commun. Lett.*, vol. 13, no. 4, pp. 227–229, Apr. 2009.

[21] Y. Ai and M. Cheffena, "Performance analysis of hybrid-ARQ with chase combining over cooperative relay network with asymmetric fading channels," in *2016 IEEE 84th Veh. Technol. Conf. (VTC-Fall)*, Sep. 2016, pp. 1–6.

[22] P. Jayasinghe *et al.*, "Performance analysis of optimal beamforming in fixed-gain AF MIMO relaying over asymmetric fading channels," *IEEE Trans. Commun.*, vol. 62, no. 4, pp. 1201–1217, Apr. 2014.

[23] H. Ju and R. Zhang, "Throughput maximization in wireless powered communication networks," *IEEE Trans. Wireless Commun.*, vol. 13, no. 1, pp. 418–428, 2014.

[24] ——, "Optimal resource allocation in full-duplex wireless-powered communication network," *IEEE Trans. Commun.*, vol. 62, no. 10, pp. 3528–3540, 2014.

[25] X. Kang, C. K. Ho, and S. Sun, "Full-duplex wireless-powered communication network with energy causality," *IEEE Trans. Wireless Commun.*, vol. 14, no. 10, pp. 5539–5551, Oct. 2015.

[26] M. Babaei, U. Aygölü, and E. Basar, "BER analysis of dual-hop relaying with energy harvesting in Nakagami-m fading channel," *IEEE Trans. Wireless Commun.*, vol. 17, no. 7, pp. 4352–4361, Jul. 2018.

[27] C. Zhong, H. A. Suraweera, G. Zheng, I. Krikidis, and Z. Zhang, "Wireless information and power transfer with Full Duplex relaying," *IEEE Trans. Commun.*, vol. 62, no. 10, pp. 3447–3461, Oct. 2014.

[28] C. Xu, M. Zheng, W. Liang, H. Yu, and Y. Liang, "End-to-end throughput maximization for underlay multi-hop cognitive radio networks with RF energy harvesting," *IEEE Trans. Wireless Commun.*, vol. 16, no. 6, pp. 3561–3572, Jun. 2017.

[29] J. Zhang and G. Pan, "Outage analysis of wireless-powered relaying MIMO systems with non-linear energy harvesters and imperfect CSI," *IEEE Access*, vol. 4, pp. 7046–7053, Oct. 2016.

[30] F. Tan, H. Chen, and F. Zhao, "Performance analysis of energy harvesting multi-antenna relaying system over mixed nakagami-m/rician fading channels," *Physical Commun. J.*, vol. 34, pp. 157–164, Jun. 2019.

[31] V. Singh and H. Ochiai, "Throughput improvement by cluster-based multihop wireless networks with energy harvesting relays," in *2017 IEEE Topical Conference on Wireless Sensors and Sensor Networks (WiSNet)*, 2017, pp. 61–64.

[32] E. Illi, F. El Bouanani, and F. Ayoub, "Physical layer security of an amplify-and-forward energy harvesting-based mixed RF/UOW system," in *2019 Int. Conf. on Adv. Commun. Tech. and Netw. (CommNet)*, 2019, pp. 1–8.

[33] L. Rubio, J. Reig, and N. Cardona, "Evaluation of Nakagami fading behaviour based on measurements in urban scenarios," *AEU - Int. J. Electron. Commun.*, vol. 61, pp. 135–138, Feb. 2007.

[34] I. S. Gradshteyn and I. M. Ryzhik, *Table of Integrals, Series, and Products: Seventh Edition*. Burlington, MA: Elsevier, 2007.

[35] N. T. Hai and S. B. Yakubovich, *The Double Mellin-Barnes Type Integrals and their Applications to Convolution Theory*. P O Box 128, Farrer Road, Singapore 9128: World Scientific Publishing Co. Pte. Ltd, 1992.

[36] E. Illi, F. E. Bouanani, and F. Ayoub, "A performance study of a hybrid 5G RF/FSO transmission system," in *Int. Conf. Wireless Net. Mobile Commun. (WINCOM)*, Nov. 2017, pp. 1–7.

[37] A. A. Kilbas and M. Saigo, *H-Transforms: Theory and Applications*. Boca Raton, Florida, US: CRC Press, 2004.

[38] P. C. Sofotasios, S. Muhaidat, M. Valkama, M. Ghogho, and G. K. Karagiannidis, "Entropy and channel capacity under optimum power and rate adaptation over generalized fading conditions," *IEEE Signal Process. Lett.*, vol. 22, no. 11, pp. 2162–2166, Nov 2015.

[39] P. S. Bithas and P. T. Mathiopoulos, "Capacity of correlated generalized Gamma fading with dual-branch selection diversity," *IEEE Trans. Veh. Technol.*, vol. 58, no. 9, pp. 5258–5663, Nov. 2009.

[40] H. A. Suraweera, D. S. Michalopoulos, and G. K. Karagiannidis, "Performance of distributed diversity systems with a single amplify-and-forward relay," *IEEE Trans. Veh. Tech.*, vol. 58, no. 5, pp. 2603–2608, Jun 2009.

[41] I. W. Research, *Mathematica Edition: version 11.3*. Champaign, Illinois: Wolfram Research, Inc., 2018.

[42] A. Mathai, R. K. Saxena, and H. J. Haubol, *The H-Function Theory and Applications*. New York: Springer, 2010.